

Charge Schedule Optimization and Infrastructure Planning for Solar-Integrated Electric Bus Transit Systems

Madhusudan Baldua^{*1}, Rito Brata Nath^{*1}, Vivek Vasudeva², and Tarun Rambha^{✉1,2}

¹Department of Civil Engineering, Indian Institute of Science (IISc), Bengaluru, India

²Center for infrastructure, Sustainable Transportation and Urban Planning (CiSTUP), Indian Institute of Science (IISc), Bengaluru, India

Abstract

As urban transit systems transition towards electrification, using renewable energy sources (RES), such as solar, is essential to make them efficient and sustainable. However, the intermittent nature of renewables poses a challenge in deciding the solar panel requirements and battery energy storage system (BESS) capacity at charging locations. To address these challenges, we propose a two-stage stochastic programming model that considers seasonality in solar energy generation while incorporating temperature-based variations in bus energy consumption and dynamic time-of-use electricity prices. Specifically, we formulate the problem as a multi-scenario linear program (LP) where the first-stage long-term variables determine the charging station power capacity, BESS capacity, and the solar panel area at each charging location. The second-stage scenario-specific variables prescribe the energy transferred to buses directly from the grid or the BESS during layovers. We demonstrate the effectiveness of this framework using data from Durham Transit Network (Ontario) and Action Buses (Canberra), where bus schedules and charging locations are determined using a concurrent scheduler-based heuristic. Solar energy data is collected from the National Renewable Energy Laboratory (NREL) database. We solved the multi-scenario LP using Benders' decomposition, which performed better than the dual simplex method, especially when the number of scenarios was high. With solar energy production at the depots, our model estimated a cost savings of 16.48% and 32.00% for the Durham and Canberra networks, respectively. Our results also show that the scenario-based schedule adapts better to seasonal variations than a schedule estimated from average input parameters.

Keywords: electric bus charge scheduling, renewable energy, linear programming, Benders' decomposition.

1 Introduction

Assessing and minimizing the carbon footprint is crucial to combat climate change. In 2019, the transport sector resulted in 8.7 gigatons of carbon dioxide equivalent (GtCO₂-eq) in direct greenhouse gas emissions, an increase of 75% from its value in 1990. The transportation sector contributes to 23% of global energy-related emissions, of which direct road transport accounted for almost 70% of emissions [1]. As per a report by the International Energy Agency [2], trucks and buses contributed to over 35% of the direct CO₂ emissions from road transport, despite making up less than 8% vehicles. Owing to this growing concern, electrification of urban transit systems has gained significant impetus over the last decade, with electric buses (EBs) emerging as a critical component of sustainable public transportation solutions. [3] reported that over 220 heavy-duty electric vehicles (EVs) models entered the market in 2022. Governments of twenty-seven countries have committed to reaching 100% zero-emission bus and truck sales by 2040.

Despite the environmental advantages of EBs, their widespread adoption is hindered by the limited energy density, short operational range, and extended recharging times. Mitigating range anxiety remains a significant challenge, especially in scenarios where EBs operate throughout the day. The introduction of opportunity fast charging [4] enables EBs to make more trips, promoting greater uptake. Charging should be done so that bus battery levels do not violate the optimal depth-of-discharge limits (DoD) [5]. Effective managing of EB fleets requires solving two main

(*) These authors contributed equally to this manuscript. (✉ tarunrambha@iisc.ac.in) Corresponding author

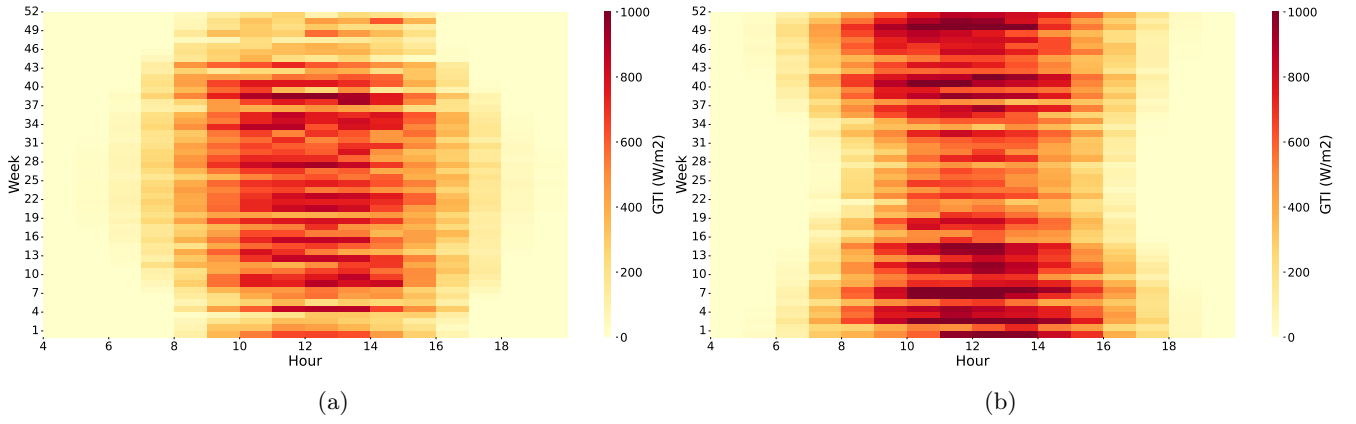


Figure 1: Weekly variations of GTI across the day for Durham (left) and Canberra (right) (Source: [NREL](#))

problems: the *Electric Vehicle Scheduling Problem* (EVSP) and the *Charge Scheduling Problem* (CSP). The EVSP is an extension of the Multi-Depot Vehicle Scheduling Problem (MDVSP), where the goal is to assign timetabled trips to vehicles to minimize fixed and operational costs without violating range restrictions. On the other hand, the CSP determines a charging schedule for electric buses that minimizes the sum of contracted power capacity costs and electricity consumption costs based on time-of-use (ToU) prices.

As the usage of EVs continues to grow, planners and system operators are concerned about maintaining the reliability of the power grid [6]. During peak demand hours, strategic integration of charging stations with renewable energy sources (RES) such as photovoltaics (PVs) can complement the grid in an environmentally friendly manner [7, 8]. For example, many cities worldwide supplement the electricity grid with sustainable energy sources [9]. Cities such as Hobart and Canberra generate all their electricity needs from renewable energy sources. Despite this, generating additional solar energy by installing PVs locally is encouraged. This can create cheaper, self-sustaining microgrids that are resilient to cascading grid failures. However, using energy from RES presents challenges due to its stochastic nature. It is susceptible to variations in climatic conditions throughout the day, month, and year, as illustrated in Figure 1 for the Durham and Canberra networks. The plot shows the Global Tilted Irradiance (GTI), a measure of the available solar energy, across the day for different weeks of the year. One can notice that the GTI values are higher in summers between 9 am and 4 pm than at other times.

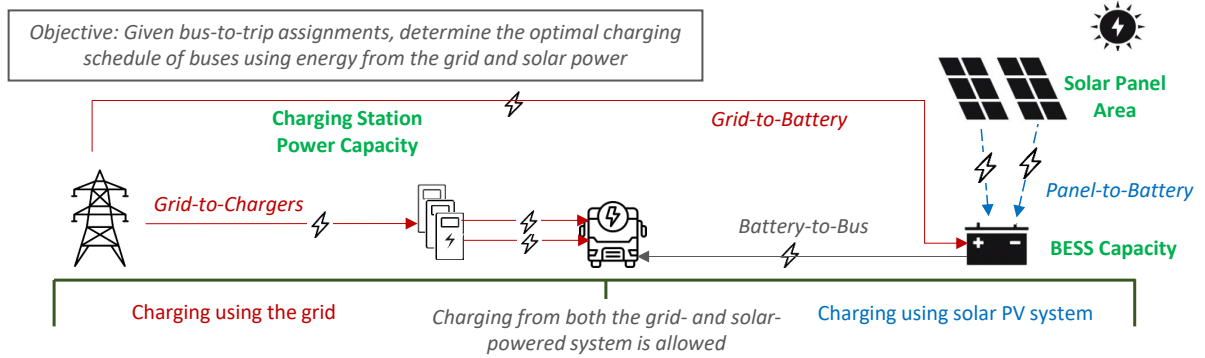


Figure 2: Illustration of a charging depot with solar panels and battery energy storage system (BESS). Green captions denote the long-term decisions, and arrows denote the operational, short-term decisions. Red- and blue-colored labels are associated with the grid and solar systems, respectively. Gray labels denote that the charging can be done using both the grid and solar PV systems.

From a consumption standpoint, the energy requirements of EBs are significantly influenced by driver behavior, charging strategies, road gradients, and battery life [10, 11]. Variations in ambient temperature also significantly impact trip energy consumption, implying that we can vary bus-to-trip assignments across the year for better system performance. Thus, finding solutions to the EVSP and the CSP requires addressing the planning and operational aspects of the charging infrastructure, keeping variations of supply and demand in mind. At a planning level, we need to decide how much grid capacity to design charging depots for, what the solar panel sizes should be, and how

much battery storage capacity to have. Figure 2 illustrates an EB depot in which buses can charge either from the grid, a solar-powered system, or both. The long-term planning decisions are marked using bold icons with green captions, and operational decisions regarding charge schedules are marked using red (grid power), blue (solar power), and gray (both grid and solar power) arrows. Depending on the realization of GTI and temperatures, in each time interval (which we refer to as a *scenario*), short-term decisions on bus-to-trip assignments and charge schedules are optimized at an operational level. This scenario-based approach helps us address the following fundamental question. *How beneficial is it to optimally integrate RES while operating electric transit fleets?* We address this question with a stylized, system-level model, simplifying some elements to ensure scalability. Furthermore, we demonstrate the importance of accounting for temperature-specific energy consumption in the CSP and explore solution techniques that make the framework computationally tractable for real-world networks. More specifically, our study makes the following contributions.

- We propose a two-stage multi-scenario linear programming (LP) model where the first-stage variables determine the long-term decisions, such as contracted grid capacity, battery capacity to store energy, and the area of solar panels installed at each charging location. The second-stage variables are associated with a specific scenario and decide the energy the BESS draws from the grid and the energy buses take from the BESS and the grid under dynamic ToU electricity prices.
- We employ a concurrent scheduler-based (CS) heuristic that optimizes bus-to-trip assignments using the energy consumption estimates while incorporating the effect of ambient temperature. This algorithm allows us to use a different number of buses in different scenarios with a fixed set of charging locations. Charge scheduling for each scenario is solved by Benders’ decomposition to improve the computational tractability for large networks.
- We analyze the benefits of RES using a case study by constructing weekly, monthly, quarterly, and yearly scenarios for two real-world networks from Durham and Canberra with 2092 and 3911 trips, respectively. Our model generates charge schedules with significant cost savings of 16.48% and 32.00% for the two networks due to the integration of depot-level RES. In addition, our model shows that ignoring ambient temperature effects can lead to an underestimation of the total cost by 27.77% and 14.92% for Durham and Canberra, respectively.

The rest of the paper is structured as follows. Section 2 presents an overview of the literature on CSP, CSP with RES, and real-world uncertainties for EBs. Section 3 outlines an EVSP solution, which uses a concurrent scheduler-based algorithm to generate bus-to-trip assignments. Section 4 provides a CSP formulation with seasonality in solar energy production and ambient temperature-based trip energy consumption. We also describe Benders’ decomposition, which is used to solve our formulation. In Section 5, we present the results of our case studies on the Durham and Canberra transit networks and highlight valuable insights. We summarize our findings in Section 6 and outline potential areas for future research. We list the abbreviations used in this paper in Appendix A.

2 Literature Review

Two main problems in managing EB fleet operations include the EVSP and the CSP. The EVSP provides a bus-to-trip assignment, whereas the CSP determines the charging schedules for EBs based on ToU electricity prices. The optimized charge schedules can also be used to decide where to open charging stations from a set of candidates. We discuss relevant literature on CSP in Section 2.1 and a summary of CSP with renewables and various sources of uncertainty in Section 2.2. An overview of EB fleet management problems can be found in [12].

2.1 Charge Scheduling Problem

The charging schedule of EBs affects the operational cost, primarily due to the variability in electricity pricing and energy demand [13]. The primary goal of the CSP is to minimize the operational cost with known bus-to-trip assignments and potential charging locations. It can account for ToU electricity prices, grid capacity, charging infrastructure capacity, and integration of RES. Apart from ToU energy tariffs, many studies have examined the impact of the EV charging schedules on power grid systems [14, 15]. Uncoordinated charging of energy-intensive EBs poses a significant challenge to the stability of the grid [16, 17, 18]. Therefore, effectively managing grid constraints while meeting state-of-charge (SoC) requirements becomes crucial [19, 20, 21].

Several studies have focused on reducing the peak load on the grid. [22] investigated the impacts of replacing diesel buses with EBs on the power grid system for the Hamburg bus depot. [23] implemented greedy heuristics to minimize peak load under centralized depot charging. [24] used non-linear programming-based methods for optimizing overnight charging decisions with battery aging costs for EB fleets. [25] formulated discrete time-based and event-based mixed-integer linear programs (MILPs) for optimizing the opportunity fast-charging schedule for a single depot. [18] and [26] imposed demand charges to compute precise charging costs while formulating mixed-integer second-order cone programming and mixed-integer non-linear programming problems, respectively. Demand charges indicate the electricity billing based on the total energy requirement from the grid within 15 minutes or one hour. [27] modeled each charger separately in their charging infrastructure and scheduling problem and proposed a bi-level optimization framework. [28] integrated location and scheduling problems by proposing split and uniform charging models based on charging priority rules while considering dynamic ToU pricing and charging station power capacity. We extend some of their CSP models in our study.

2.2 Renewables and Uncertainties

Economic and environmental benefits of EBs hinge on the effective integration of RES for either complete or partial vehicle charging [29]. A review of models for smart charging of EVs using PVs and ToU pricing can be found in [30]. Energy storage systems are a potential solution to reduce high electricity demand charges at charging locations [31, 32]. Recent studies have focused on such integrated systems. [20] integrated wind energy sources into the power grid, and [11] focused on a PV-based charging station with BESS to optimize the overall operational cost for bus and parking agencies, respectively. [33] explored the cost potential of EBs by considering their bus-to-grid capabilities to sell electricity back to the grid. [34] utilized a genetic algorithm to optimize charging and discharging schedules for the Penghu bus transportation system, considering factors such as solar and wind power generation, feeder load, and demand response. [35] addressed uncertainties related to PV systems and building load patterns by employing 15-minute long short-term memory predictions. Their objective was to minimize the overall cost of workplace-integrated microgrids. [36] explored a system with PVs, BESS, a diesel generator, and grid-connected charging stations to ensure constant and uninterrupted charging, whereas [37] proposed a system in which EBs are equipped with rooftop solar panels to provide on-board energy supply. To address the uncertainty in solar energy generation, [38] used chance-constrained LPs and [39] proposed a two-stage multi-objective planning framework to coordinate the scheduling of EVs, BESS, and PVs at a charging station. [40] addressed the charging location planning problem, and [41] addressed the charge scheduling problem integrated with PV and BESS using an MILP model.

[42] modeled the uncertainty in the EV arrival rates as a Markov process with variable grid power prices at different periods. Similarly, to address the energy consumption variability during bus operations, [43] developed stochastic energy management strategies at charging stations. Their approach involved a distributionally robust Markov Decision Process (MDP) with RES. [44] formulated a two-stage stochastic program with a hybrid charging scheme, which was solved using a progressive hedging algorithm. [45] proposed a stochastic two-stage multi-objective model for charging and discharging schedules of EBs to minimize the depot operator’s energy and battery degradation costs. To enhance tractability, [46] used Benders’ decomposition on a two-stage stochastic model for an intelligent grid, which addresses variations in demand response, RES, EVs, and market prices. Likewise, [47] used Benders’ decomposition to solve the charging infrastructure and scheduling problem using renewables. However, they simplified their model by combining trips based on charging time-window availability and considered only three scenarios for PV generation.

Due to the sporadic nature of RES, determining the appropriate battery storage capacity and the solar panel capacity at a station poses a significant challenge. The fluctuating energy production and trip energy requirements significantly impact daily charge schedules. A practical approach to dealing with these variations involves considering a range of possible scenarios and their associated probabilities of occurrence. Findings from [48] indicate that deploying PVs and BESS at charging stations using a synchronized charging schedule is a practical choice for handling peak loads. We address a similar CSP problem that can deal with variations in the energy consumption of the EBs and RES availability.

Table 1 compares features of our work with existing literature. Although studies related to RES in the context of EVs are abundant, literature on EBs integrated with RES is scarce. The schedules of EVs requiring charging at a depot are challenging to predict. Hence, most studies that integrate EV operations with RES assume random arrivals of EVs at a charging station [42, 29]. For EBs, the timetable is fixed by transit operators, so it is possible to plan strategically and determine the exact itinerary for each bus. However, the intermittent nature of RES remains a challenge in integrated systems. To our knowledge, no study has tackled the CSP with seasonal solar energy

Table 1: Model features in relevant works on EB charge scheduling (1: Grid Capacity, 2: Solar Infrastructure, 3: Partial Charging, 4: BESS, 5: RES, 6: Uncertainty/Seasonality, 7: Model/Solution Technique, 8: Problem Scale (we report only the number of EBs when the trip information is not available), ◦ not clear in the paper, blank spaces represent features that are not modeled)

| Ref. | (1) | (2) | (3) | (4) | (5) | (6) | (7) | (8) |
|-----------------|-----|-----|-----|-----|-----|-------------------------------------|--|---------------------|
| [25] | • | | • | | | | MILP | 47 EBs |
| [48] | • | ◦ | | • | • | | MILP and charge scheduling algorithm | 144 trips, 24 EBs |
| [44] | ◦ | | | | | Energy consumption | Progressive hedging algorithm | 6 EBs |
| [34] | • | • | • | ◦ | • | | Genetic algorithm | 29 EBs |
| [20] | • | | • | | • | Charging energy | Monte Carlo simulation | 17 trips, 10 EBs |
| [49] | • | | ◦ | | | | MILP | 11 EBs |
| [47] | • | • | ◦ | • | • | Solar energy | Benders' decomposition | 316 trips, 10 EBs |
| [45] | • | • | | • | • | EB schedule | MILP | 50 EBs |
| [46] | • | ◦ | | • | • | Power system | Benders' decomposition | 180 EBs |
| [43] | • | ◦ | | • | • | Energy consumption | Distributionally robust MDP and heuristics | Not clear |
| Our Work | • | • | • | • | • | Energy consumption and solar energy | Benders' decomposition | 3911 trips, 265 EBs |

generation and variable bus-to-trip assignments for EBs. Our study bridges this gap by proposing a multi-scenario LP formulation, which is solved using Benders' decomposition [50]. Readers can refer to [51] for a detailed review of Benders' decomposition. Most studies in Table 1 do not model solar infrastructure and battery storage capacity decisions. In addition to capturing these features, we consider partial bus charging through a split charging model using grid- and solar-powered systems. Another unique aspect of our study is the scale of the problems addressed. The largest network used in our research includes 265 EBs, serving 3911 daily trips. Furthermore, a high number of scenarios makes our problem more practical. Before delving into our problem formulation, we present some background on EVSP in Section 3.

3 Preliminaries

Transit operations are characterized by routes/lines and trips carried out on each route. The timetable for trips is assumed to be fixed and is repeated daily. When the fleet contains EBs, operators must also identify charging locations and charging schedules and assign buses to trips. Two typical charging methods include overnight depot charging and within-day opportunity charging. We assume that overnight depot charging replenishes bus batteries to the same energy level daily, keeping charging schedules periodic and simplifying managerial decisions. Opportunity fast charging is done during the day to meet the energy needs of buses and to ensure that the battery levels of buses stay higher than the minimum threshold. Terminals where many trips originate or end are chosen as depots for overnight charging. Chargers are made available at such locations, and we assume that buses charge overnight at the depots after their daily operations. Depot chargers can also be used for opportunity charging during the day. In addition, non-depot terminals serve as candidate locations for installing opportunity chargers. Buses are assumed to start their journey at a depot, serve one or more trips during the day, and return to the same depot at the end of the day. We assign buses to trips based on trip compatibility and energy requirements. Two trips i_1 and i_2 are compatible if a bus can serve trip i_2 after serving trip i_1 . This is possible if the end time of trip i_1 plus the time to deadhead from the end-stop of i_1 to the start-stop of i_2 is less than or equal to the start time of trip i_2 .

A *scenario* or a time interval can be based on different levels of aggregation such as weeks, months, quarters, or a year and is characterized by two properties – GTI values and ambient temperatures across different times of the day. The GTI values are used to decide the amount of energy generated from solar power in each scenario. Ambient temperature variations, on the other hand, influence the energy consumption for service and deadheading trips. Due to the differences in energy consumption for the same trip across scenarios, we also employ different EVSP assignments for different scenarios. The literature on the electric bus-to-trip assignment problem or the EVSP is abundant. EVSP is an extension of the MDVSP that can be formulated either as a multi-commodity flow model or a set partitioning model [52, 53] and is an NP-hard problem [54]. Researchers have tackled the EVSP using MILP models and column generation for small-sized networks [55]. Heuristics such as genetic algorithms [56], simulated annealing [57], and adaptive large neighborhood search [58] have also been used to solve large instances.

Table 2: Notation used in the CS algorithm

| Notation | Description |
|------------------------------------|---|
| Index: | |
| b | Bus index |
| ω | Index of a scenario |
| Sets/Lists: | |
| I | Set of trips (an individual trip is indexed by i) |
| D | Set of depots |
| W | Set of scenarios |
| V^ω | List of rotations of all the EBs for scenario ω |
| V | List of rotations of all the EBs for all scenarios, i.e., $(V_\omega)_{\omega \in W}$ |
| V_b^ω | Rotation of b^{th} electric bus in scenario ω |
| J | Set of charging locations for all scenarios, including the depots |
| J^ω | Set of charging locations for scenario ω including the depots |
| A^{comp} | Set of compatible trip pairs |
| E^ω | List of energy requirements for service and deadheading trips for scenario ω , i.e., $[(d_i^\omega)_{i \in I}, (d_{i,l}^\omega)_{i \in I, l \in D}, (d_{i,l}^\omega)_{i \in D, l \in I}, (d_{i,l}^\omega)_{i \in I, l \in I}]$ |
| Data: | |
| i_b^l | l^{th} trip performed by bus b |
| Δ_i | Nearest depot location from the starting bus stop location of trip $i \in I$ |
| n | Number of trips in the timetable |
| n_b | Number of trips performed by bus b |
| d_i^ω | Energy consumed (in kWh) on trip i in scenario ω |
| $d_{i,l}^\omega$ | Energy (in kWh) for deadheading from the end-stop of i to the start-stop of l in scenario ω |
| i^{start} | Starting stop of trip i |
| i^{end} | Ending stop of trip i |
| ρ | Current energy level (in kWh) of a bus |
| $\delta_{i_b^l, i_b^{l+1}}^\omega$ | Time available for charging between the end of l^{th} trip and start of $(l+1)^{\text{th}}$ trip in bus b 's rotation in scenario ω |
| Parameters: | |
| ρ_{max} | Maximum battery capacity (kWh) of the bus up to which it can be charged |
| ρ_{min} | Minimum battery capacity (kWh) of the bus below which it cannot be discharged |
| μ | Maximum amount of energy (kWh/min) that can be transferred to the bus either from the power grid or from the BESS in any time step |

Our scenario-specific bus schedule or *rotations* and the initial set of charging locations are generated using a CS-based heuristic [59, 28], which only focuses on the feasibility of bus charging and does not specifically integrate solar-powered systems. We present a modified version of the approach discussed in [28] in Algorithm 1. Refer to Table 2 for notation. For a given scenario ω , the algorithm starts by initializing the set of charging locations to the set of depots (line 2). The service trips are then sorted in ascending order of their start times (line 3). A new bus rotation is created by assigning the first trip to the bus, which we assume is always charge feasible (line 5). The algorithm prioritizes inserting trips from the sorted list of service trips to a bus rotation in use (lines 7–13) based on trip compatibility (line 8) and charging level feasibility (line 10). The feasibility of the bus energy levels is verified using the ISROTATIONCHARGEFEASIBLE function, which takes the current bus rotation, charging locations, and the scenario-specific energy consumption as inputs.

We present a pseudocode for this function in Algorithm 2. Charge feasibility checks and modifications to the charging locations are performed based on a *Charge-and-Go* (CAG) strategy [28] where we prioritize charging a bus at the end-stop of a trip instead of the start-stop of the subsequent trip. If the trip insertion (lines 11–13) is not feasible, we create a new bus rotation (lines 14–15) and assign the trip to it. The scenario-specific bus rotations and initial charging locations are inputs to our CSP model, which will be explained in Section 4. The union of all scenario-specific charging locations is treated as the set of initial charging locations for the CSP (line 16).

Figure 3 illustrates the operation of a bus with five service trips, a deadheading trip between two service trips, and charging opportunities 1, 2, and 3. A *charging opportunity* arises if a bus has a layover at a charging station (which could also be a depot) either at the end of a trip or at the beginning of a trip. During this layover, the bus may charge, deadhead, or remain idle. Charging opportunities typically occur at a terminal equipped with charging stations or at the depot during overnight hours.

Algorithm 1: CONCURRENTSCHEDULER(CS)

Input: $I, D, W, E^\omega \forall \omega \in W$ **Output:** $J, V^\omega \forall \omega \in W$

```
1 for  $\omega \in W$  do
2    $V^\omega, J^\omega \leftarrow \emptyset, D$ 
3   Rearrange  $I$  in the ascending order of the trip start times
4   Pick the first trip  $i$  from the sorted list of  $I$ 
5    $V_1^\omega \leftarrow [\Delta_i, i, \Delta_i]$  and add  $V_1^\omega$  to  $V^\omega$ 
   // Add trips to existing rotations
6   for  $l = 2$  to  $n$  do
7      $i_l \leftarrow$  The  $l^{\text{th}}$  element from the sorted list of  $I$ 
8     for  $b = 1$  to  $|V^\omega| : (i_b^{nb}, i_l) \in A^{comp}$  do
9        $V_b^{temp} \leftarrow V_b^\omega$  and insert  $i_l$  to the list of service trips in  $V_b^{temp}$ 
10      insertTrip,  $J^{temp} \leftarrow \text{ISROTATIONCHARGEFEASIBLE}(V_b^{temp}, J^\omega, E^\omega)$ 
11      if insertTrip then
12         $V_b^\omega \leftarrow V_b^{temp}$  and  $J^\omega \leftarrow J^{temp}$ 
13      break
   // Create new rotations
14   if  $i_l$  is not assigned to any of the buses used so far then
15     Use a new bus  $|V^\omega| + 1$ , update its rotation to  $[\Delta_{i_l}, i_l, \Delta_{i_l}]$ , and add it to  $V^\omega$ 
16  $J \leftarrow \bigcup_{\omega \in W} J^\omega$ 
```

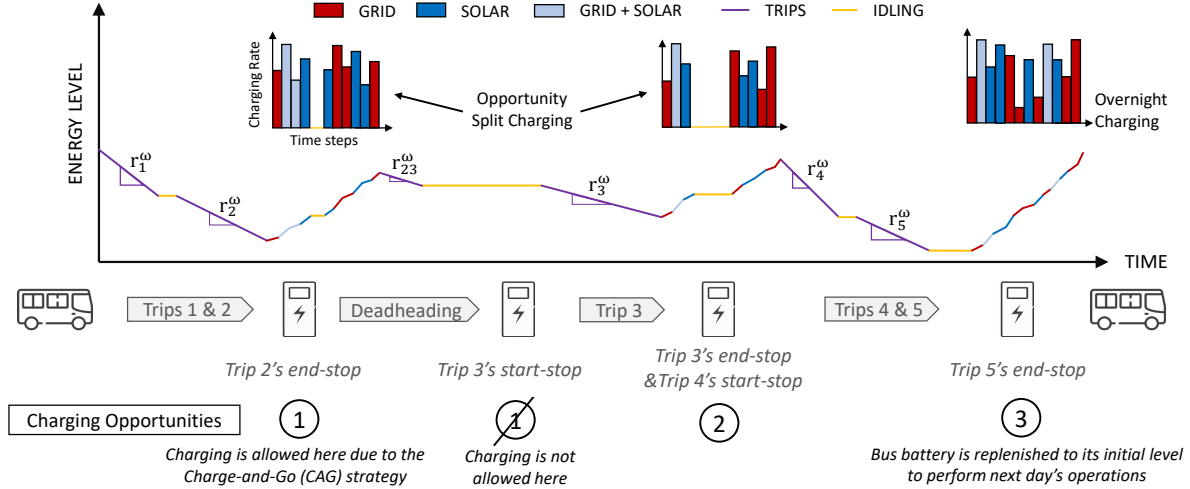


Figure 3: Charging operations for a bus showing energy levels during trips (purple), charging through grid (red), solar (dark blue) or both (light blue), and idling (yellow)

The figure illustrates that charging opportunities 1 and 2 occur between service trips, whereas overnight charging occurs during charging opportunity 3. The energy levels for the service trips are marked in purple; charging activities are shown in red (grid-powered), dark blue (solar-powered), and light blue (both grid- and solar-powered); and idling after trips or during charging opportunities is depicted in yellow. Note that solar-powered charging indicates that the bus is solely charged using solar energy, and the BESS has no residual energy left from the grid.

The figure also illustrates the CAG charging strategy for a bus where the operator encounters a dilemma to either charge at the end-stop of trip 2 or the start-stop of trip 3 when charging stations are available at both places. The CAG strategy assumes that charging opportunity 1 is assigned to trip 2's end-stop instead of trip 3's start-stop. The bus charges at charging opportunity 1 and deadheads to the start-stop of the next trip, arriving exactly at its departure time. This assumption helps eliminate additional decisions on when buses should deadhead to the next

trip's start location and allows casting the CSP as an LP instead of an MILP, thus improving its tractability. We assume that charging rates may vary over time, as shown in the plots at the upper level of the figure. In other words, the energy supplied during a charging opportunity may be split non-uniformly. The energy consumption rate for service and deadheading trips (see $r_1^\omega, r_2^\omega, r_{23}^\omega, \dots, r_5^\omega$) can vary depending on the average ambient temperature during the trip, its length, and travel time. Note that the slopes are related to d_i^ω and $d_{i,l}^\omega$ mentioned in Table 2. In practice, the energy consumption rates for a service/deadheading trip need not be constant. We simplify it in our model since these rates have no bearing on the CSP decisions.

Algorithm 2: ISROTATIONCHARGEFEASIBLE

Input: V_b^{temp}, J, E^ω
Output: True/False, J

```

1  $\rho \leftarrow \rho_{max} - d_{i_b^0, i_b^1}^\omega - d_{i_b^1}^\omega$ 
2 if  $\rho < \rho_{min}$  then return false,  $J$ 
3 for  $l = 1$  to  $(n_b - 1)$  do
    // Current trip end is a charging station
4 if  $i_b^{l,end} \in J$  then
5      $\rho \leftarrow \min\{\rho_{max}, \rho + \mu \delta_{i_b^l, i_b^{l+1}}^\omega\} - d_{i_b^l, i_b^{l+1}}^\omega$ 
    // Only next trip start is a charging station
6 if  $i_b^{l,end} \notin J, i_b^{l+1,start} \in J$  then
7      $\rho \leftarrow \min\{\rho_{max}, \rho - d_{i_b^l, i_b^{l+1}}^\omega + \mu \delta_{i_b^l, i_b^{l+1}}^\omega\}$ 
    // Current trip end and next trip start are not charging stations
8 if  $i_b^{l,end} \notin J, i_b^{l+1,start} \notin J, \rho - d_{i_b^l, i_b^{l+1}}^\omega - d_{i_b^{l+1}}^\omega \geq \rho_{min}$  then
9      $\rho \leftarrow \rho - d_{i_b^l, i_b^{l+1}}^\omega$ 
10 if  $i_b^{l,end} \notin J, i_b^{l+1,start} \notin J, \rho - d_{i_b^l, i_b^{l+1}}^\omega - d_{i_b^{l+1}}^\omega < \rho_{min}$  then
    // Open a new charging station at the current trip end to meet the charging requirement
11      $\rho \leftarrow \min\{\rho_{max}, \rho + \mu \delta_{i_b^l, i_b^{l+1}}^\omega\} - d_{i_b^l, i_b^{l+1}}^\omega$ 
    // Update the charging locations if the next trip can be performed after charging
12     if  $\rho - d_{i_b^{l+1}}^\omega \geq \rho_{min}$  then  $J \leftarrow J \cup \{i_b^{l,end}\}$ 
13      $\rho \leftarrow \rho - d_{i_b^{l+1}}^\omega$ 
14 if  $\rho < \rho_{min}$  then return false,  $J$ 
15  $\rho \leftarrow \rho - d_{i_b^{n_b}, i_b^{n_b+1}}^\omega$ 
16 if  $\rho < \rho_{min}$  then return false,  $J$ 
17 return true,  $J$ 

```

In the concurrent scheduler-based algorithm, checking the charge level feasibility for buses while inserting a trip to an existing bus rotation is paramount for generating feasible rotations. This check is performed by Algorithm 2, which takes the bus rotation, current charging locations, and the energy consumption of service and deadheading trips for the given scenario as inputs. The algorithm first checks if the bus can be charged at the end-stop of the current trip, provided a charging station is located there (lines 4–5). If not, it proceeds to check if the start-stop of the next trip is a charging location and whether the bus can charge there (lines 6–7). If neither of the above two conditions are met, the bus proceeds to perform the next trip, provided it does not run out of energy (lines 8–9). If not, a charging location is opened at the current trip end according to the CAG strategy (lines 10–12). A charging station is opened only if the bus can complete the next trip by charging at the maximum rate during the layover (line 12). The algorithm also checks the energy level of the bus after the completion of the next trip (lines 13–14) and the deadheading trip to the depot (lines 15–16). The algorithm returns a boolean variable indicating the bus rotation's charge feasibility and the charging stations' updated configuration. The pseudocode presented here is slightly abridged for ease of explanation. In the experiments, when terminal stops are clustered, we allow buses to deadhead to a nearby charging location within a cluster.

Here is an example to illustrate the workings of Algorithm 2. Consider the bus rotation in Figure 4. The rotation has five service trips $\{1, \dots, 5\}$. Assume that (a) the minimum and maximum charge levels for the bus are 50 kWh and

250 kWh, respectively, (b) each trip consumes 40 kWh, (c) each deadheading move between two consecutive trips consumes 10 kWh, (d) the bus starts with an initial charge of 200 kWh, and (e) the EVSP solution allows increasing the charge level by up to 30 kWh at a charging location, and (f) the existing charging locations are at 1^{end} , 2^{start} , and 4^{start} . The number above the nodes indicates the charge level of the bus when it arrives at that location. When the bus reaches 1^{end} , its charge level is 160 kWh. Since charging is available at 1^{end} , the algorithm requires the bus to be charged at that location, bringing the charge level to 190 kWh. No charging is done at 2^{start} because of the CAG strategy. Note that other bus rotations can use the charging station at 2^{start} . When the bus reaches 4^{start} after two service trips and three deadheading moves, the charge level reduces to 80 kWh. Since a charging facility is available at 4^{start} , the charge level gets updated to 110 kWh at 4^{start} and 70 kWh when the bus reaches 4^{end} . Since the bus requires 50 kWh to deadhead and finish trip 5, the charge level would drop below the minimum threshold. Hence, the algorithm suggests opening a new charging station at 4^{end} , making the bus rotation charge feasible.

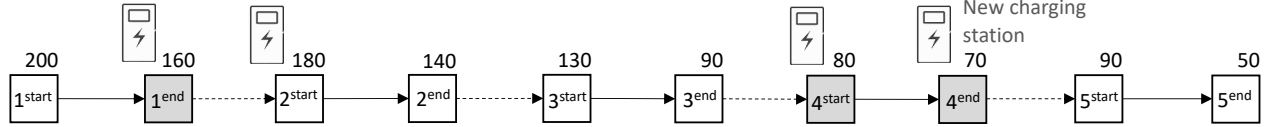


Figure 4: Example to illustrate Algorithm 2. The numbers next to nodes indicate the charge levels upon reaching it. Gray nodes represent locations where the bus charges according to the CAG strategy.

4 Scenario-based Charge Scheduling Problem

This section presents an LP model for the scenario-based CSP with dynamic ToU electricity prices, temperature-based energy consumption, and renewable energy production at charging locations. For each scenario, we divide the time horizon of operations within a day into one-minute time steps. A charging opportunity can encompass multiple time steps in which the bus can be charged from the grid, BESS, or both, and the energy drawn from either source is considered a decision variable. We also decide the energy transferred from the grid to the BESS at every time step. The scenario-based LP formulation is presented in Section 4.1, and the Benders' decomposition approach is outlined in Section 4.2. We make the following assumptions in the CSP, some of which can be trivially relaxed. We also discuss how we obtain estimates for the generated solar energy and the trip energy consumption values under different scenarios.

Assumptions:

- The CSP is optimized by the bus agency, which covers the initial investment cost for the contracted station power capacity, solar panels, BESS, and associated inventory.
- Availability of a sufficient number of chargers is assumed at the charging locations, i.e., we do not explicitly model charger assignment. Instead, we focus on estimating the aggregate power needs at a charging location. Such locations are assumed to be equipped with smart charging technology, which allows split charging [60].
- Buses are charged from the BESS or the grid. BESS can charge and discharge simultaneously. The maximum energy that can be transferred per minute from the grid and the BESS to a bus is assumed to be the same [61]. The BESS is assumed to be charged both from solar power and the grid [62]. BESS cannot be fully discharged as we assume a 90% DoD [63] for batteries.
- All buses are homogeneous and have sufficient charging opportunities to complete daily operations. They can be partially charged multiple times with a piecewise-linear charging profile, as seen in Figure 3. To allow continuity in operations, we assume that a bus starts and ends its schedule at the same depot.
- We assume that the fleet size prescribed by the CS-based algorithm is adequate for serving trips across all scenarios. As the energy consumption per trip varies across scenarios, the number of buses required may also differ. Buses may be redistributed across depots for different scenarios (i.e., across weeks, months, etc.) through rebalancing if needed.

- Sufficient space for solar panel installation is assumed at the charging locations. If the panel area requirement is too high, panels can be installed on the rooftops of nearby buildings, or additional constraints can be imposed in the model. The energy transfer from the panel to BESS happens instantaneously [64].

Energy Consumption Estimates: The energy consumption per trip is estimated using a linear regression equation from [65] as follows:

$$\text{Energy per trip } i \text{ (in kWh)} = \exp(\alpha_0 + \alpha_1 \log L_i + \alpha_2 \log M_i + \alpha_3 \log t_i + \alpha_4 |\bar{T}_i - \bar{T}_g^*|) \quad (1)$$

where L_i is the length (in km) of trip i , M_i is the mass (in kg) of the EB serving trip i , t_i is the travel time (in minutes) of trip i , \bar{T}_i (in $^{\circ}\text{C}$) is the average ambient temperature during trip i , \bar{T}_g^* (in $^{\circ}\text{C}$) is the optimum working temperature of the EB, and $\alpha_0, \dots, \alpha_4$ are estimated linear regression parameters. The ambient temperature for a trip is calculated by averaging the historical temperature values at its start and end stops. We used the same value of M_i across all trips. With additional ridership data, a more realistic estimate of the energy consumed during a trip can be obtained.

Solar Energy Estimates: The solar energy per minute is estimated using the following equation from [66]:

$$\text{Energy per minute (in kWh/min)} = \text{GTI} \times \text{Panel Area} \times \frac{\eta}{100} \times \frac{1}{60} \quad (2)$$

where GTI is in kW/m^2 , Panel Area is in m^2 , and η is in %.

4.1 Formulation

Table 3 summarizes the notation used in the CSP model. The long-term decision variables determine the power capacity (z_j), solar panel area (a_j), the BESS capacity (c_j), and the initial energy level for the BESS (d_j) for every charging location j . The scenarios-specific daily operational decisions include determining the energy transferred from the grid ($x_{b,j,t}^{\omega}$) and BESS ($y_{b,j,t}^{\omega}$) to every bus b , and the energy transferred from the grid to BESS ($h_{j,t}^{\omega}$) at charging location j and time step t within each day for scenario ω . Additionally, auxiliary variables are used to track the energy level ($u_{b,k}^{\omega}$) of bus b after charging opportunity k , and the energy level of BESS ($v_{j,t}^{\omega}$) at charging location j and time step t for scenario ω .

To illustrate the sets used in the CSP formulation, consider the network shown in the left panel of Figure 5, which depicts eight trips covered by three buses. The stops $s_1 \dots, s_8$ indicate the end terminals of the trips. The numbers next to the links represent the trip travel times, and the numbers next to the nodes in boxes denote the layover times between trips, respectively. Note that the layover times for different trips ending at the same stop are identical. Additionally, we assume that the three buses start their journey simultaneously. Charging facilities are present at stops s_2 and s_4 , marked in gray. Bus 1 covers four trips—(s_1, s_2), (s_2, s_3), (s_3, s_4), and (s_4, s_5); bus 2 covers two trips—(s_6, s_2) and (s_2, s_7); and bus 3 covers two trips—(s_8, s_4) and (s_4, s_9). Bus 1 has two charging opportunities at s_2 and s_4 . Buses 2 and 3, on the other hand, have a single charging opportunity at s_2 and s_4 , respectively. The bus schedule is shown in the Gantt chart in the right panel of Figure 5 for a scenario ω . For the CSP, we need to keep track of events that occur at the charging stations. Table 4 provides the information on the set of buses present at each location in different time steps, $B^{\omega}(j, t)$, and the time steps corresponding to different charging opportunities for each bus, $T^{\omega}(b, k)$.

The objective function (3) for the CSP consists of six terms. The first three terms represent the per day cost of the BESS capacity, the contracted station power capacity, and the installed solar panel area, respectively. These decisions are related to the bus agency's long-term initial investments. The last three terms are expected values of scenario-specific terms: the first for the energy drawn from the grid to the buses, the next for the energy sourced by the buses from the BESS, and the final for the energy transferred from the grid to the BESS. The objective denotes the daily average cost. The occurrence of each scenario is equally likely since we assume that the scenarios correspond to time intervals of equal duration. We use a life-cycle of 12 years for BESS [67, 68] and the bus battery charging systems [69], and 30 years for the solar panels [70], which is reflected in the constants used in the objective function.

Table 3: Notation used in the CSP formulation

| Index: | Description |
|-----------------------------|---|
| t | Index for a within-day time step |
| k | Index for charging opportunity |
| j | Index for location |
| Sets: | |
| B^ω | Set of buses for scenario ω |
| T^ω | Set of time steps for scenario ω , where each day's operations are discretized at a one-minute granularity. |
| $K^\omega(b)$ | Set of charging opportunities for bus b for scenario ω |
| $B^\omega(j, t)$ | Set of buses present at location j in time step t for scenario ω |
| $T^\omega(b, k)$ | Set of time steps for which bus b can charge at its k^{th} charging opportunity for scenario ω either from the power grid or BESS |
| Decision Variables: | |
| $x_{b,j,t}^\omega$ | Energy (in kWh/min) transferred from the grid to the bus b at charging location j in time step t for scenario ω |
| $y_{b,j,t}^\omega$ | Energy (in kWh/min) transferred from the BESS to the bus b at charging location j in time step t for scenario ω |
| $h_{j,t}^\omega$ | Energy transferred (in kWh/min) from the grid to the BESS at charging location j in time step t for scenario ω |
| z_j | Charging station power capacity (in kW) at location j |
| a_j | Total solar panel area (in m^2) installed at location j |
| c_j | BESS capacity (in kWh) at charging location j |
| d_j | Energy level (in kWh) of the BESS at location j at the start and end of daily operations across all scenarios |
| Auxiliary Variables: | |
| $u_{b,k}^\omega$ | Energy level (in kWh) of bus b before the start of its $(k+1)^{\text{th}}$ charging opportunity for scenario ω |
| $v_{j,t}^\omega$ | Energy level (in kWh) of the BESS at charging location j at the end of time step t for scenario ω |
| Data: | |
| $j_{b,k}$ | Location of bus b at its k^{th} charging opportunity |
| $g_{j,t}^\omega$ | GTI values (in kWh/ m^2) at charging location j in time step $t \in T^\omega$ for scenario ω |
| $e_{b,k}^\omega$ | Energy required (in kWh) by bus b after its k^{th} charging opportunity to complete the subsequent service and deadheading trips until its $(k+1)^{\text{th}}$ charging opportunity for scenario ω . This is calculated using d_i^ω and $d_{i,l}^\omega$. |
| p^ω | Probability of the occurrence of scenario ω |
| τ_b^ω | Last charging opportunity for bus b under scenario ω |
| m_j^ω | Time step corresponding to the end of daily operations at location j for scenario ω (to track BESS's energy level). We set this value to 1440. |
| Parameters: | |
| ϵ_t^ω | Grid ToU electricity price per unit energy (in \$/kWh) in time step t for scenario ω |
| σ | Unit solar energy price (in \$/kWh) |
| π | Unit cost of solar-powered battery (in \$/kWh) |
| γ | Unit cost of charging station power capacity (in \$/kW) at potential charging locations |
| α | Cost of solar panel per unit area (in \$/ m^2) |
| η | Efficiency (%) of solar panels |
| DoD | DoD of BESS |

Table 4: Buses present at a charging location over time and time steps for charging opportunities in the example shown in Figure 5

| Location (j) | s_2 | s_2 | s_2 | s_2 | s_4 | s_4 | s_4 | s_4 | s_4 |
|------------------------------|---------|-------|-------|------------|-------|---------|-------|------------|-------|
| Time (t) | 4 | 5 | 6 | 7 | 10 | 11 | 12 | 13 | 14 |
| $B^\omega(j, t)$ | {2} | {1,2} | {1,2} | {1} | {3} | {3} | {1,3} | {1} | {1} |
| Bus (b) | 1 | | | 1 | | 2 | | 3 | |
| Charging Opportunity (k) | 1 | | | 2 | | 1 | | 1 | |
| $T^\omega(b, k)$ | {5,6,7} | | | {12,13,14} | | {4,5,6} | | {10,11,12} | |

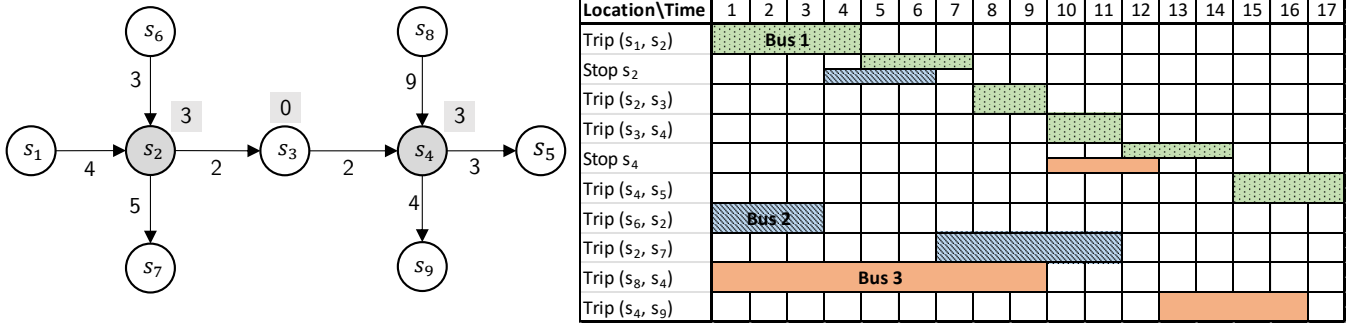


Figure 5: Example network (left panel) and Gantt chart (right panel) illustrating the data for the CSP

$$\min \frac{\pi}{365 \times 12} \sum_{j \in J} c_j + \frac{\gamma}{365 \times 12} \sum_{j \in J} z_j + \frac{\alpha}{365 \times 30} \sum_{j \in J} a_j + \sum_{\omega \in W} p^\omega \left(\sum_{b \in B^\omega} \sum_{\substack{k \in K^\omega(b), \\ t \in T^\omega(b,k), j'=j_{b,k}}} (\epsilon_t^\omega x_{b,j',t}^\omega + \sigma y_{b,j',t}^\omega) + \sum_{j \in J} \sum_{t \in T^\omega} \epsilon_t^\omega h_{j,t}^\omega \right) \quad (3)$$

$$\text{s.t. } u_{b,k}^\omega = u_{b,k-1}^\omega - e_{b,k}^\omega + \sum_{t \in T^\omega(b,k)} (x_{b,j',t}^\omega + y_{b,j',t}^\omega) \quad \forall \omega \in W, b \in B^\omega, k \in K^\omega(b), j' = j_{b,k} \quad (4)$$

$$u_{b,k-1}^\omega + \sum_{t \in T^\omega(b,k)} (x_{b,j',t}^\omega + y_{b,j',t}^\omega) \leq \rho_{max} \quad \forall \omega \in W, b \in B^\omega, k \in K^\omega(b), j' = j_{b,k} \quad (5)$$

$$v_{j,t}^\omega = v_{j,t-1}^\omega + \frac{\eta g_{j,t}^\omega a_j}{60} + h_{j,t}^\omega - \sum_{b \in B^\omega(j,t)} y_{b,j,t}^\omega \quad \forall \omega \in W, j \in J, t \in T^\omega \quad (6)$$

$$c_j \geq v_{j,t-1}^\omega + \frac{\eta g_{j,t}^\omega a_j}{60} + h_{j,t}^\omega \quad \forall \omega \in W, j \in J, t \in T^\omega \quad (7)$$

$$v_{j,t}^\omega \geq (1 - DoD) c_j \quad \forall \omega \in W, j \in J, t \in T^\omega \quad (8)$$

$$\sum_{b \in B^\omega(j,t)} 60 x_{b,j,t}^\omega + 60 h_{j,t}^\omega \leq z_j \quad \forall \omega \in W, j \in J, t \in T^\omega \quad (9)$$

$$x_{b,j',t}^\omega + y_{b,j',t}^\omega \leq \mu \quad \forall \omega \in W, b \in B^\omega, k \in K^\omega(b), t \in T^\omega(b,k), j' = j_{b,k} \quad (10)$$

$$u_{b,k}^\omega \geq \rho_{min} \quad \forall \omega \in W, b \in B^\omega, k \in K^\omega(b) \quad (11)$$

$$u_{b,0}^\omega = u_{b,\tau_b^\omega}^\omega \quad \forall \omega \in W, b \in B^\omega \quad (12)$$

$$v_{j,0}^\omega = v_{j,m_j^\omega}^\omega = d_j \quad \forall \omega \in W, j \in J \quad (13)$$

$$x_{b,j',t}^\omega \geq 0, y_{b,j',t}^\omega \geq 0 \quad \forall \omega \in W, b \in B^\omega, k \in K^\omega(b), t \in T^\omega(b,k), j' = j_{b,k} \quad (14)$$

$$a_j \geq 0, c_j \geq 0, z_j \geq 0, d_j \geq 0 \quad \forall j \in J \quad (15)$$

$$h_{j,t}^\omega \geq 0 \quad \forall \omega \in W, j \in J, t \in T^\omega \quad (16)$$

All the constraints except (15) in our formulation are dependent on the scenarios. Constraint (4) tracks the energy level of each bus at the end of every charging opportunity. It is not necessary to monitor the energy level at every time step, and doing so would also significantly increase the number of decision variables. Constraint (5) ensures that buses do not charge above their battery's maximum capacity. Constraint (6) tracks the energy level of the BESS for all locations. Constraint (7) models the maximum capacity of the BESS. Constraint (8) sets the lower bound of the energy level of BESS based on its DoD. Constraint (9) determines the power capacity of charging locations by calculating the peak energy requirements. Constraint (10) restricts the maximum energy transferred to the bus from the power grid or BESS in any time step. Constraint (11) ensures that the SoC of the bus battery never drops below a minimum level. Constraint (12) sets the initial energy level of each bus b to the energy level at the end of the operations to implement recurring schedules in each scenario. Charging opportunity indices 0 and τ_b^ω represent the

overnight charging opportunities on the previous and the current day, respectively. (Charging opportunity indexing in Figures 3 and 5 starts from 1 since the overnight charging activity on the previous day is not shown.) Constraint (13) similarly equates the starting energy level of batteries on a given day to that on the subsequent day. This ensures consistent initialization across all scenarios to facilitate transitions from one scenario to another. Finally, constraints (14), (15), and (16) require variables to be non-negative.

Given the variation in the available solar energy and temperature-based trip energy consumption across scenarios, scenario-based optimization helps us make better long-term decisions. However, as we increase the number of scenarios, the number of variables and constraints increases, making it difficult to solve the LP for larger networks using the simplex method. Since the constraint matrix has a block diagonal structure, this problem is a good candidate for applying Benders' decomposition.

4.2 Benders' Decomposition

The formulation discussed previously in (3)–(16) has a two-stage structure in which the contracted grid capacity, solar-powered BESS capacity, the area of solar panels, and the energy levels of the BESS that needs to be maintained at the start and end of operations are decided in the first stage. Fine-grained charging decisions are made in the second stage, adapting to the scenario-specific GTI and temperature values. The constraints for this problem can be represented using (17), which has a block diagonal shape with non-overlapping blocks for each scenario, except for the first-stage variables that appear in every scenario.

$$\begin{bmatrix} A_{00} & & & & \\ A_{10} & A_{11} & & & \\ A_{20} & & A_{22} & & \\ \vdots & & & \ddots & \\ A_{\phi 0} & & & & A_{\phi \theta} \end{bmatrix} \begin{bmatrix} \lambda_0 \\ \lambda_1 \\ \lambda_2 \\ \vdots \\ \lambda_\theta \end{bmatrix} = \begin{bmatrix} \beta_0 \\ \beta_1 \\ \beta_2 \\ \vdots \\ \beta_\phi \end{bmatrix} \quad (17)$$

Benders' decomposition or the L-shaped method is ideal for improving the tractability of two-stage recourse models, especially when the number of scenarios is high [71]. In this approach, one creates a *restricted main/parent problem* containing only constraints with first-stage variables. The objective for the restricted main problem includes the long-term variables and a term for each *sub-problem* or *child problem*, which indicates the current assessment (or a lower bound) of the sub-problem's objective. A solution to the restricted main problem allows us to fix the first-stage decisions, which results in an independent sub-problem for each scenario. However, a scenario-specific sub-problem might not be feasible for the current values of the first-stage variables. In such a case, one can use duality theory to obtain a feasibility cut from the sub-problem and add it to the restricted main problem. Alternatively, the main problem's assessment of the objective function value of the scenario-specific sub-problem could be less than the actual objective value of the sub-problem. In this case, we add an optimality cut from the sub-problem to the restricted main problem. The method iteratively solves the restricted main problem and the sub-problems until the main problem does not lead to a feasibility or an optimality cut from any sub-problem.

To apply Benders' decomposition for the CSP, we can formulate the objective function of the main problem as (18) where ζ^ω is the assessment of the objective value of the second stage for scenario ω . Thus, $\sum_{\omega \in W} p^\omega \zeta^\omega$ denotes the average contribution of the second-stage decisions in the overall objective. In our formulation, the first-stage problem contains only non-negativity constraints (15) in the first iteration. Additional location-specific capacity or budgetary constraints involving the first-stage variables can be easily incorporated if needed.

$$\min \left(\frac{\pi}{365 \times 12} \sum_{j \in J} c_j + \frac{\gamma}{365 \times 12} \sum_{j \in J} z_j + \frac{\alpha}{365 \times 30} \sum_{j \in J} a_j \right) + \sum_{\omega \in W} p^\omega \zeta^\omega \quad (18)$$

After solving (18) subject to (15), the values of the first-stage variables (represented with additional bars) are fixed in each scenario-based LP as shown below for a scenario ω .

$$\min \sum_{b \in B^\omega} \sum_{\substack{k \in K^\omega(b), \\ t \in T^\omega(b, k), j' = j_{b, k}}} (\epsilon_t^\omega x_{b, j', t}^\omega + \sigma y_{b, j', t}^\omega) + \sum_{j \in J} \sum_{t \in T^\omega} \epsilon_t^\omega h_{j, t}^\omega \quad (19)$$

s.t. (4), (5), (10), (11), (12), (14), (16) for scenario ω

$$v_{j,t}^\omega - v_{j,t-1}^\omega + \sum_{b \in B^\omega(j,t)} y_{b,j,t}^\omega - h_{j,t}^\omega = \frac{\eta g_{j,t}^\omega \bar{a}_j}{60} \quad \forall j \in J, t \in T^\omega \quad (20)$$

$$v_{j,t-1}^\omega + h_{j,t}^\omega \leq \bar{c}_j - \frac{\eta g_{j,t}^\omega \bar{a}_j}{60} \quad \forall j \in J, t \in T^\omega \quad (21)$$

$$v_{j,t}^\omega \geq (1 - DoD)\bar{c}_j \quad \forall j \in J, t \in T^\omega \quad (22)$$

$$\sum_{b \in B^\omega(j,t)} 60 x_{b,j,t}^\omega + 60 h_{j,t}^\omega \leq \bar{z}_j \quad \forall j \in J, t \in T^\omega \quad (23)$$

$$v_{j,0}^\omega = v_{j,m_j}^\omega = \bar{d}_j \quad \forall j \in J \quad (24)$$

If a scenario-based LP is infeasible, a feasibility cut is added to the first-stage problem. On the other hand, if the LP is feasible but has an objective (19) that is not close enough to ζ^ω , then an optimality cut is added to the first-stage problem. As discussed earlier, utilizing this iterative approach improves tractability. The following section presents a case study to demonstrate its advantages.

5 Experiments and Results

Our experiments were run on two real-world bus transit networks using a Dell Precision workstation with AMD Ryzen Threadripper Pro 7975WX CPU @ 4.0 GHz and 256 GB of RAM. The LP models were implemented in Python 3.10 with CPLEX 22.1.1. We used CPLEX’s built-in Benders’ decomposition implementation with our annotations for the variables and benchmarked it against CPLEX’s (dual simplex) LP solver. The maximum time limit for both models was set to 24 hours for each instance. The source codes are available on GitHub at [transnetlab/csp-res](https://github.com/transnetlab/csp-res).

5.1 Dataset and Parameters

We tested our models on the Durham Transit Network, Ontario, Canada, and Action Buses, Canberra, Australia. The General Transit Feed Specification (GTFS) data for the test networks was collected from [Transit Feeds](#). Our model requires agency-specific input data, such as fleet characteristics, potential charging locations, and depots. However, in the absence of such data, we made reasonable assumptions, where necessary, to demonstrate the advantages of our framework. The actual operations in these cities may, however, differ. Using the calendar file and service IDs, we filtered the highest number of service trips occurring on a weekday and assumed that these trips repeat daily throughout the year. Since EBs require overnight charging, we only considered trips that started before 10 pm for Durham and before 11 pm for the Canberra network to allow buses sufficient time to recharge their batteries before the next day’s operation. Alternatively, one could use extra buses to complete the overnight trips and recharge them during the daytime.

Distances between bus stops were calculated using [Open Source Routing Machine](#), which was also used to calculate the trip and deadheading distances. For deadheading, a constant speed of 30 km/hr was assumed. We considered the specifications of Ride’s [K9M-40](#) EB model for our study. To estimate the energy consumed during a trip using (1), we assumed that buses carry 50% of their passenger capacity. We formed clusters of terminal stops within a radius of 500 m to limit the number of charging locations. For each cluster, we chose the stop with the maximum number of trips passing through it as a candidate charging location.

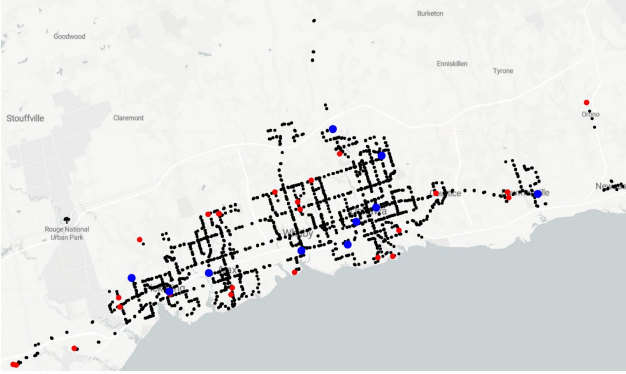
We gathered time-stamped GTI and temperature data at transit stops from PVWatts, a module developed by [NREL](#), which also required the latitude and longitude of the charging station, tilt, and array azimuth angle for installed solar panels. We assumed that the tilt value equals a location’s latitude and the array azimuth angle is 180°. We calculated the power generation per unit area for Durham and Canberra using data from [72] and [73], respectively, and used these values to convert the solar panel costs to \$/m² based on [74]. The data used in our experiments are summarized in Table 5 and were converted to per-day equivalents during implementation to scale long- and short-term model parameters. Table 6 presents the ToU electricity prices obtained from Alectra Utilities [75] (Durham) and Australian Energy Regulator [76] (Canberra).

Table 5: Parameter values

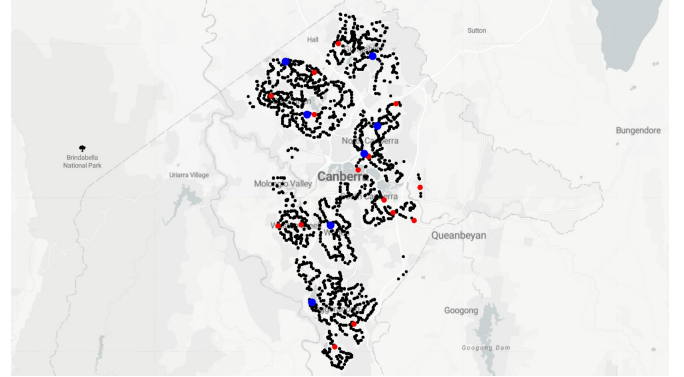
| Parameter | Value | Reference | Remark/Assumptions |
|---------------------------------|--------------------------|---------------------|---|
| σ | 0 | | Free solar energy |
| ρ_{max} | 266.05 kWh | K9M-40, [77] | 85% battery capacity |
| ρ_{min} | 46.95 kWh | K9M-40, [78] | 15% battery capacity |
| η | 20% | [79] | Photovoltaic panel efficiency |
| μ | 2.5 kWh/min | [23, 61] | Allowed energy transfer rate to buses |
| π | 500 \$/kWh | [80] (pg.5) | 12 years life span [67, 68] |
| γ | 654 \$/kW | [81] | 12 years life span [69] |
| α | 305.89 \$/m ² | [74] (pg.28, pg.32) | 30 years life span [70] (panels, inverter, maintenance) |
| DoD | 90% | [63] | DoD of BESS |
| Mass of EB | 16,121.14 kg | K9M-40 | Curb weight and 50% passenger load |
| $\alpha_0, \alpha_1, \alpha_2$ | -8.11, 0.55, 0.78 | [65] | Estimated parameters for the energy consumption profile |
| $\alpha_3, \alpha_4, \bar{T}_g$ | 0.35, 0.008, 23.3°C | [65] | |

Table 6: ToU electricity pricing (Sources: [75, 76])

| Network | Period | Peak Hours | Mid Peak/Shoulder Hours | Off Peak/Overnight Hours |
|----------|-------------------------|-----------------------|-------------------------|--------------------------|
| Durham | May–October | 11 am–5 pm | 7 am–11 am, 5 pm–7 pm | 7 pm–7 am |
| | November–April | 7 am–11 am, 5 pm–7 pm | 11 am–5 pm | 7 pm–7 am |
| | Rate (\$/kWh) (May–Oct) | 0.1219 | 0.0817 | 0.0583 |
| | Rate (\$/kWh) (Nov–Apr) | 0.1059 | 0.0817 | 0.0509 |
| Canberra | All year | 7 am–5 pm | 5 pm–10 pm | 10 pm–7 am |
| | Rate (\$/kWh) | 0.2439 | 0.1993 | 0.1647 |



(a) Durham transit network



(b) Canberra transit network

Figure 6: Stops (black), depots (blue), and opportunity charging locations (red). Note that the depots, marked blue, are also charging locations in our model.

5.2 Case Study

Our study considered 1, 4, 12, and 52 scenarios with GTI and ambient temperature data averaged across yearly, quarterly, monthly, and weekly time scales, respectively. Temperature and GTI values were available at an hourly granularity; therefore, average values were computed for each hour across the days in the scenario, and the same hourly value was assigned to every minute within that hour. We also analyzed the benefits of introducing renewable energy sources and studied the effect of temperature-specific energy consumption estimates on fixed and operating costs. While implementing the CSP solution, if a transit operator encounters a week with weather conditions that deviate from those in the model, they can either reoptimize the CSP based on short-term weather forecasts or apply the solution from a closely matching scenario.

5.2.1 Network Details

Information regarding stops, terminals, depots, routes, trips, and charging locations (obtained from Algorithm 1) for Durham and Canberra networks is given in Table 7. Figure 6 shows the charging location information for these networks.

Table 7: Network details

| Network | Stops | Terminal Stops | Depots Used | Charging Locations | Routes | Trips |
|----------|-------|----------------|-------------|--------------------|--------|-------|
| Durham | 1890 | 52 | 10 | 36 | 32 | 2092 |
| Canberra | 2423 | 67 | 7 | 24 | 65 | 3911 |

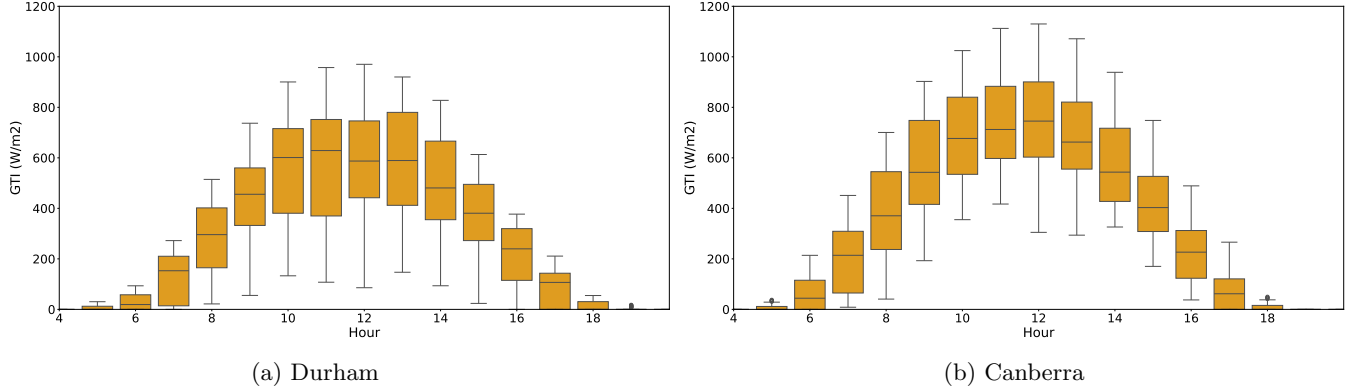


Figure 7: Box plot of GTI variations across different hours of the day

Variations in GTI values across scenarios and time-of-day for both networks are illustrated in Figures 1 and 7, respectively. Note that seasonal changes (refer Figure 1) in the southern hemisphere are opposite to those in the northern hemisphere. The grid heat map (Figure 1) highlights variations across weeks/scenarios; box plots (Figure 7) indicate the quartile range variations for a given hour. Figure 8 highlights the temperature variations in the two cities. Specifically, grid heat maps in Figures 8a and 8d show the variations in temperature across scenarios (ranging from -10 to 25 $^{\circ}\text{C}$ for Durham and from 3 to 33 $^{\circ}\text{C}$ for Canberra), which in turn result in different energy requirements for the same trip depending on the scenario.

Figures 8b and 8e show the variations in trip energy requirement when scenarios are built by averaging the temperature data over weekly, monthly, quarterly, or yearly time intervals. The energy needs for the longest trip can vary from 27 to 36 kWh for Durham (trip 181) and 21 to 25 kWh for Canberra (trip 307). This, in turn, affects the requirements for the number of EBs (see Figures 8c and 8f) and their corresponding trip assignments across scenarios. The number of required EBs was found to vary from 111 to 123 for Durham and 245 to 265 for Canberra.

5.2.2 Scenario-Based Results

Table 8 shows the optimum objective values and computation times from our experiments. For small instances, dual simplex is quick. However, as the number of scenarios increases, Benders' decomposition solves the problem faster. Dual simplex could not find a feasible solution for Durham and Canberra networks with 52 scenarios in 24 hours. The performance of Benders' decomposition depends on the tolerances of the optimality and feasibility cuts. We use the default tolerances (10^{-6}) in CPLEX for all instances except for the 52-scenario case, where we set it to 0.1. For both networks, the objective values increase with the number of scenarios, highlighting cost underestimation if sufficient scenarios are not considered. One of the reasons for this underestimation is that the model misses out on critical scenarios that influence long-term decision-making.

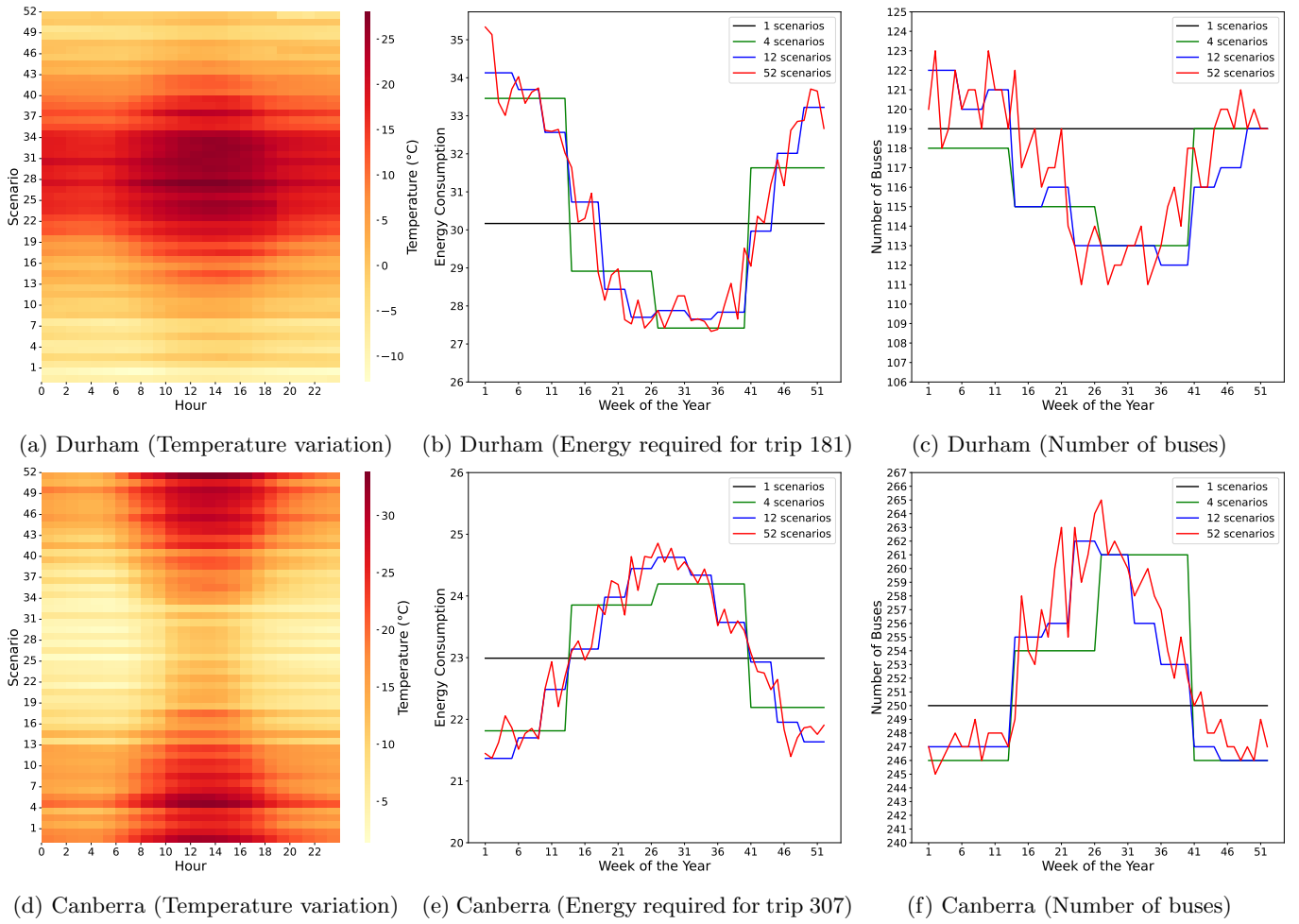


Figure 8: Hourly temperature variation (left), trip energy requirement variations (middle), and total buses required (right) across different scenarios

Table 8: Summary of results for the test networks. The numbers in bold indicate the highest cost across scenarios.

| Network | Durham | | | | Canberra | | | |
|-------------------------------|---------------|---------|---------|---------------|----------------|---------|---------|----------------|
| Scenarios | 1 | 4 | 12 | 52 | 1 | 4 | 12 | 52 |
| Variables (millions) | 0.27 | 1.07 | 3.21 | 13.99 | 0.41 | 1.67 | 4.99 | 21.78 |
| Constraints (millions) | 0.29 | 1.17 | 3.50 | 15.21 | 0.31 | 1.27 | 3.80 | 16.55 |
| Benders' runtime (minutes) | 33.22 | 62.72 | 178.81 | 648.25 | 78.20 | 188.22 | 402.50 | 1138.42 |
| Simplex runtime (minutes) | 0.89 | 30.53 | 574.67 | 1440 | 0.18 | 65.00 | 895.29 | 1440 |
| Benders' objective (\$) | 950.15 | 1161.18 | 1166.88 | 1247.12 | 3507.64 | 5128.74 | 5419.96 | 6286.33 |
| Simplex objective (\$) | 950.15 | 1161.18 | 1166.88 | — | 3507.64 | 5128.72 | 5419.96 | — |
| Contracted capacity cost (\$) | 84.64 | 173.24 | 156.46 | 179.49 | 0 | 318.23 | 321.61 | 468.73 |
| Solar panel cost (\$) | 404.99 | 319.47 | 303.46 | 241.00 | 1196.22 | 973.23 | 893.37 | 497.28 |
| BESS cost (\$) | 60.85 | 56.53 | 57.42 | 57.10 | 2311.42 | 2050.47 | 1978.49 | 298.72 |
| Average operation cost (\$) | 399.67 | 611.84 | 649.54 | 769.53 | 0 | 1786.81 | 2226.49 | 5021.60 |

When the number of scenarios is small, the installed solar panels dominate the charging station power requirements, and hence, the contracted capacity costs are low. Conversely, as the number of scenarios increases with a shorter time interval for each scenario, the grid power capacity requirement increases to handle the extreme cases of low solar energy generation, reducing the requirement for solar panels. Note that for the 4-scenario case in Canberra, the Benders' objective value is slightly higher than the dual simplex objective. This happens due to the tolerances used in the optimization solver.

5.2.3 Effect of Introducing RES and Temperature-Based Trip Energy Estimates

We also explored a 52-week scenario model with/without RES and with/without considering the effects of temperature variations in energy estimates. Table 9 summarizes the results. In both networks, considering renewables and BESS prove to be more cost-effective, as seen from the third and fourth columns of the table. Without RES, all energy is sourced from the grid, which is expensive. Note that the total energy requirements vary slightly between the two cases. This variation is due to the lower solar energy costs and deadheading of buses to charging stations within a cluster of terminals. When RES is available, buses may deadhead to a charging location that uses PVs and BESS, thereby avoiding direct charging from the grid at a higher electricity price. Due to RES, significant cost savings of 16.48% and 32.00% are achieved for the Durham and Canberra networks, respectively.

We also evaluated the optimal costs for a model with RES, ignoring the impacts of temperature on the trip energy estimates, and found that the overall cost is underestimated. This difference can be attributed to the temperature component in (1), which is set to the optimal operating temperature in the no-temperature variation case, leading to an underestimation of the total energy requirements and, consequently, a reduction in operational costs. When temperature variations are neglected, we underestimate the total costs by 27.77% and 14.92% for the two networks.

Table 9: Results quantifying the benefits of RES and temperature-based trip energy estimates. The numbers in bold represent objective values, which are the total daily costs.

| Network | Metrics | With temperature effects | | Ignoring temperature |
|----------|---------------------------------|--------------------------|----------------|----------------------|
| | | With RES | Without RES | With RES |
| Durham | Objective (\$) | 1247.12 | 1493.29 | 976.04 |
| | Average operational cost (\$) | 769.53 | 1221.51 | 554.94 |
| | Contracted capacity cost (\$) | 179.49 | 271.78 | 122.08 |
| | Solar panel cost (\$) | 241.00 | 0 | 251.02 |
| | BESS cost (\$) | 57.10 | 0 | 48.00 |
| | Total energy requirements (MWh) | 1047.16 | 1043.88 | 878.46 |
| Canberra | Objective (\$) | 6286.33 | 9243.94 | 5470.08 |
| | Average operational cost (\$) | 5021.60 | 8450.50 | 4283.41 |
| | Contracted capacity cost (\$) | 468.73 | 793.44 | 402.75 |
| | Solar panel cost (\$) | 497.28 | 0 | 486.89 |
| | BESS cost (\$) | 298.72 | 0 | 297.03 |
| | Total energy requirements (MWh) | 2426.43 | 2420.73 | 2202.54 |

5.3 Extended Analysis

While underestimating grid capacity can lead to power shortage/failure during operations, overestimating solar panel area can lead to excessive power generation that would be wasted if BESS capacity is insufficient. Figures 9 and 10 display charging location capacities, solar panel areas, and battery storage capacities necessary for optimal operations across different scenarios for Durham and Canberra networks, respectively. Since Algorithm 1 is a greedy approach and the second-stage decisions are optimized in the CSP, many charging locations (52.77% for Durham and 12.5% for Canberra) obtained through the CS-based heuristic are redundant. The charging location labels on the x-axis represent the terminal bus stop indices used for the grid- or solar-powered system. Some stops are not shown in both figures because buses do not charge at those locations.

Interestingly, overnight charging requirements primarily dominate the contracted grid power capacity. Energy from the grid was drawn predominantly by the depots, as evident from the top panel in Figures 9 and 10. All opportunity charging at non-depots was done using BESS. This pattern can be attributed to continuous solar energy generation during the daytime, the lower solar energy costs compared to the ToU grid electricity prices, and the ability to store grid energy in the BESS at a lower cost.

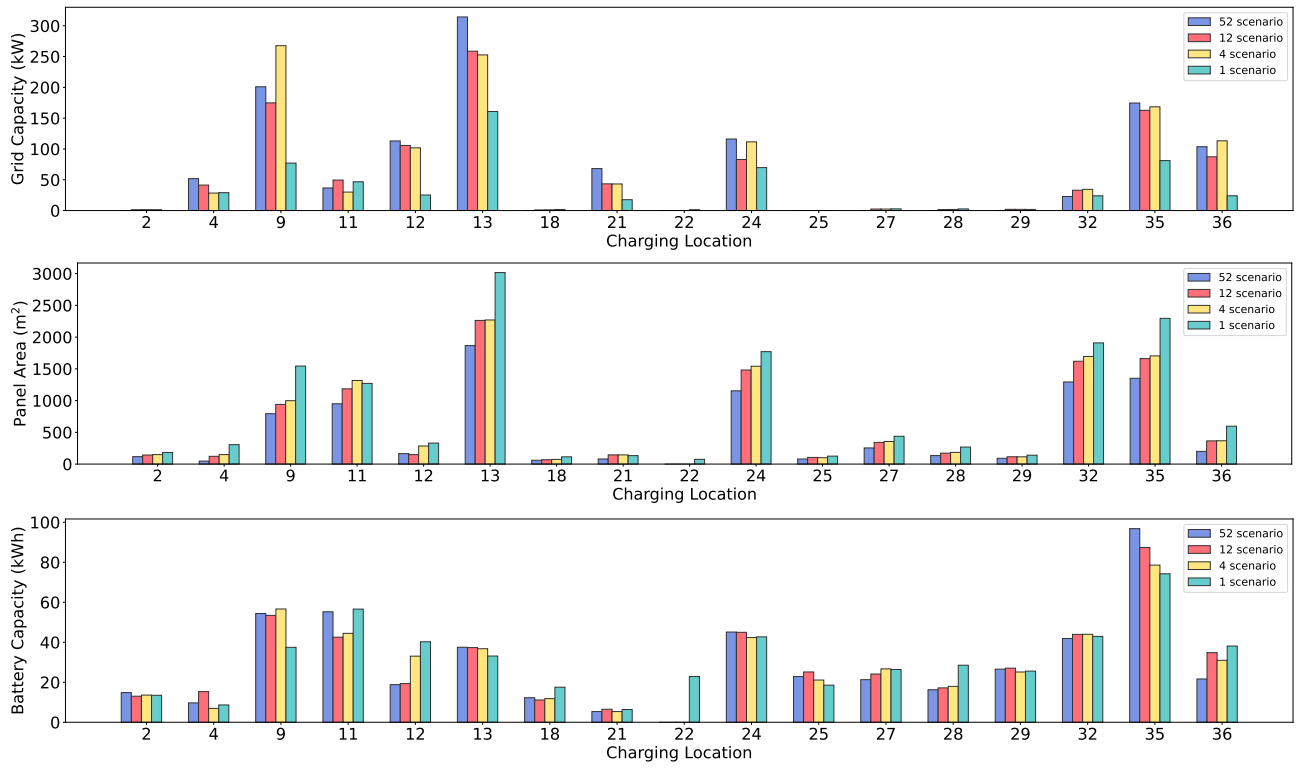


Figure 9: Contracted grid capacity (top), solar panel area (middle), and BESS capacity (bottom) for the Durham network

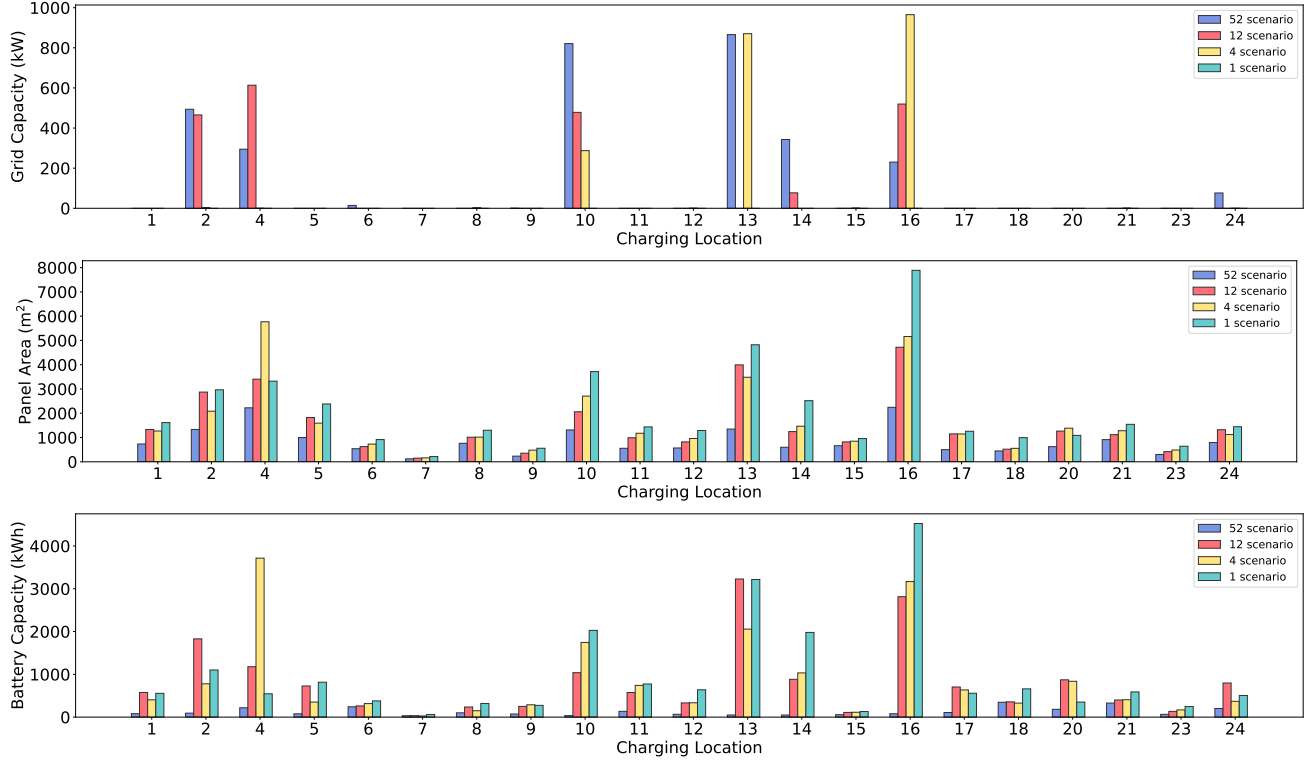


Figure 10: Contracted grid capacity (top), solar panel area (middle), and BESS capacity (bottom) for the Canberra network

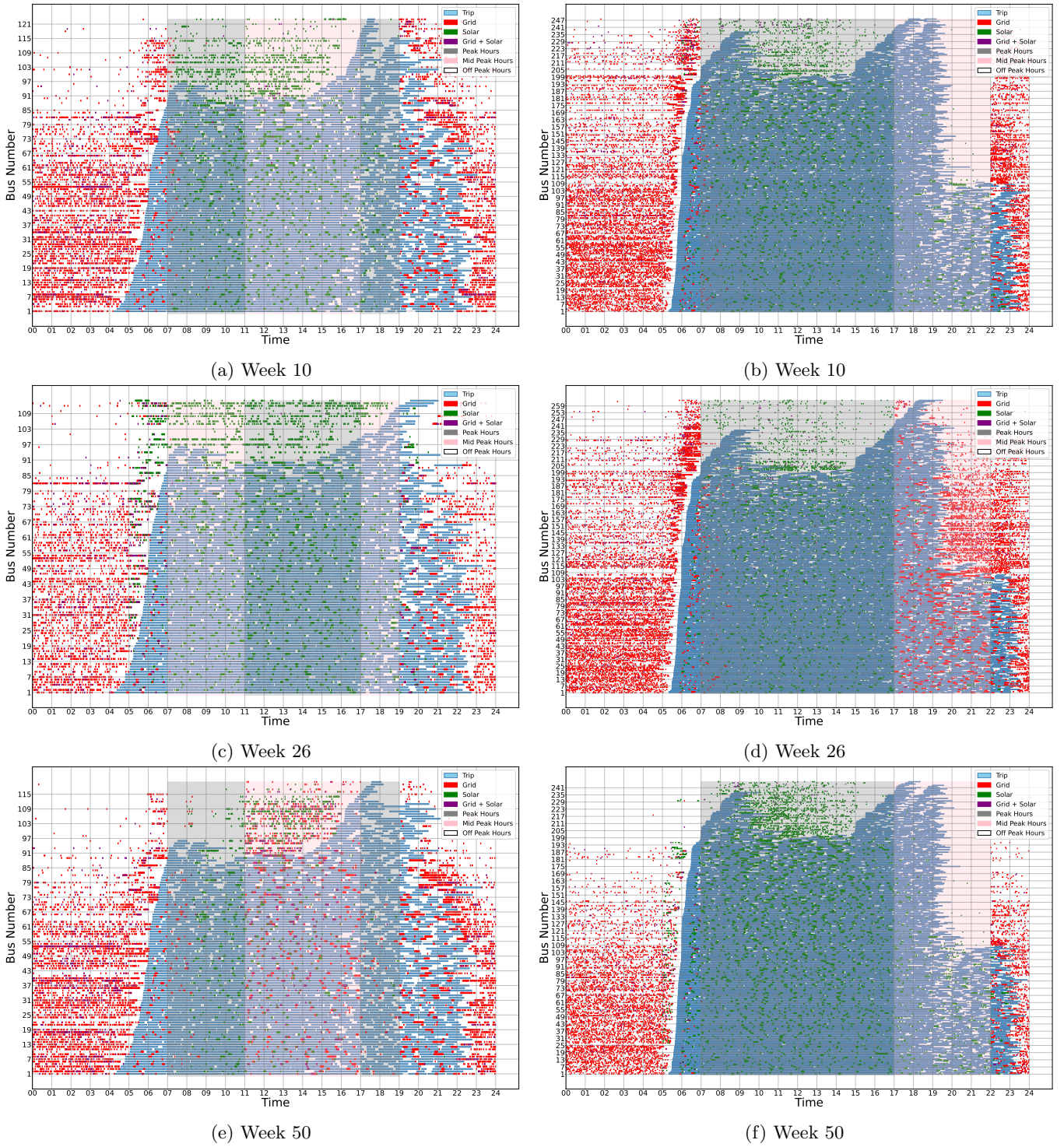
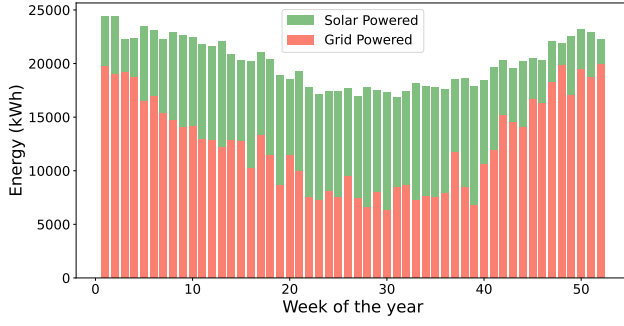
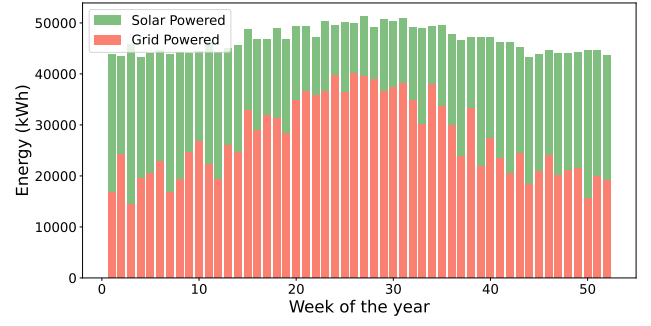


Figure 11: Bus operation schedule for Week 10, 26, and 50 (left: Durham, right: Canberra)

As discussed earlier, for both networks, as the number of scenarios decreases, the grid capacity gets underestimated, and the solar panel area is overestimated. Therefore, modeling decisions for shorter time intervals, i.e., incorporating more scenarios (52 in our case) to capture diverse climate conditions, is essential for obtaining a realistic picture of costs. We observed no discernible trends in battery storage capacity across the scenarios. However, it can be noted that the depots require higher BESS capacity than other terminals. The maximum grid capacity, panel area, and BESS capacity for Durham are 314.31 kW, 1866.80 m², and 96.79 kWh, respectively. The corresponding variables for the Canberra network are 865.70 kW, 2244.66 m², and 347.55 kWh. These long-term decisions on grid and solar



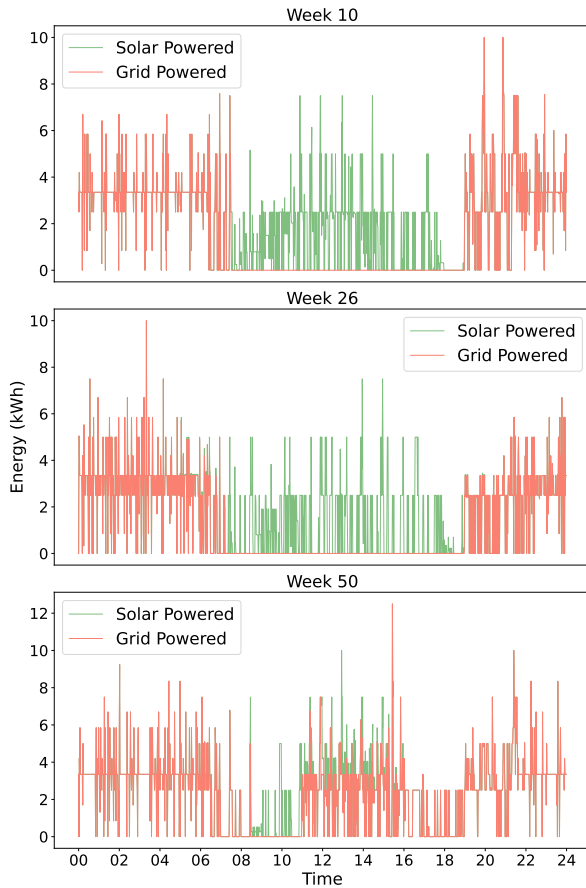
(a) Durham



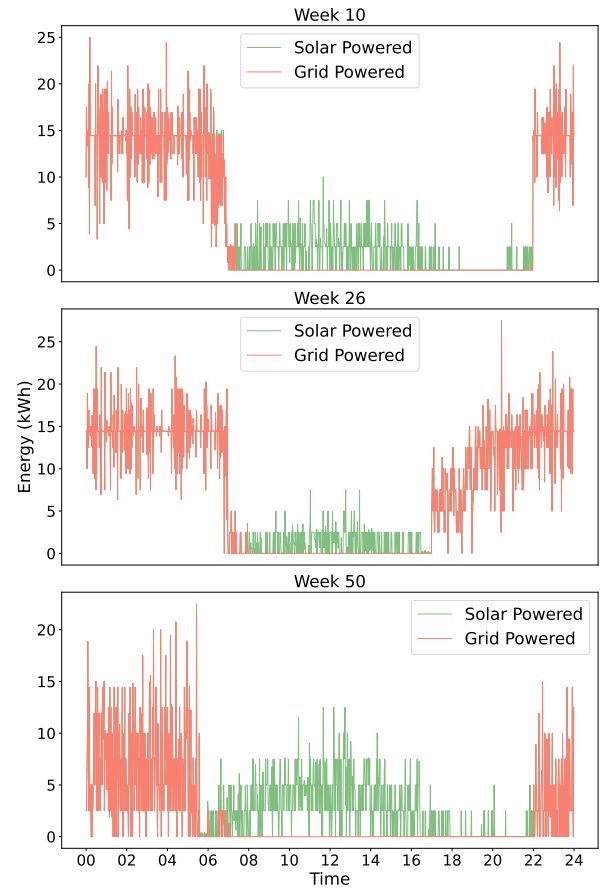
(b) Canberra

Figure 12: Energy distribution from grid and RES across different scenarios

capacity requirements were found to be within practical limits. Additionally, for the 52-scenario case, the maximum energy transfer rates from the grid to BESS are 5.24 kWh/min and 14.44 kWh/min for the Durham and Canberra networks. These values are also within the limits prescribed in the literature [82, 83].



(a) Durham – (Location 9)



(b) Canberra – (Location 13)

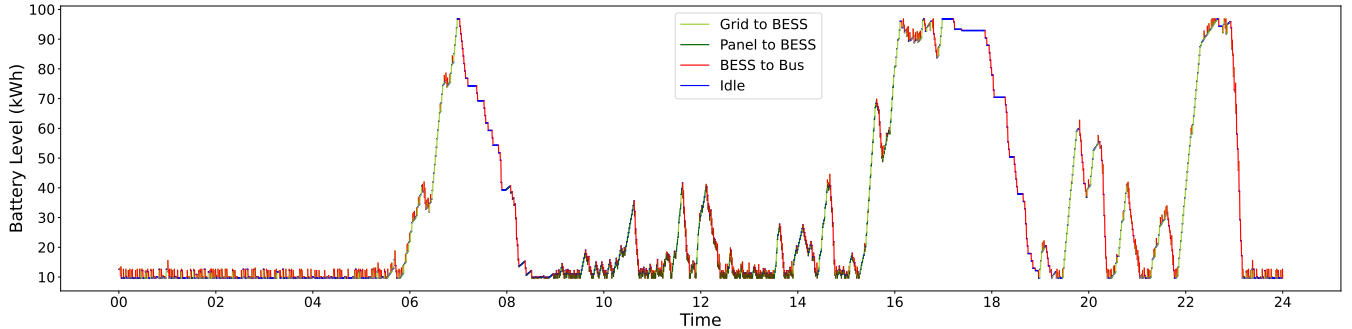
Figure 13: Scenario-wise energy utilization for weeks 10, 26, and 50 for Durham (left) and Canberra (right)

For the 52-scenario model, we focus on the results of three distinct scenarios (Weeks 10, 26, and 50) to visualize the impact of incorporating renewables, BESS, and ToU electricity prices. Figure 11 illustrates the Gantt chart schedules for these weeks/scenarios. These charts indicate trips in blue, grid-powered charging events (direct or through the BESS) in red, solar-powered charging events through the BESS in green, and grid and solar-powered charging events that happen within the same minute in purple. We find the split of grid/solar charging from the BESS through a

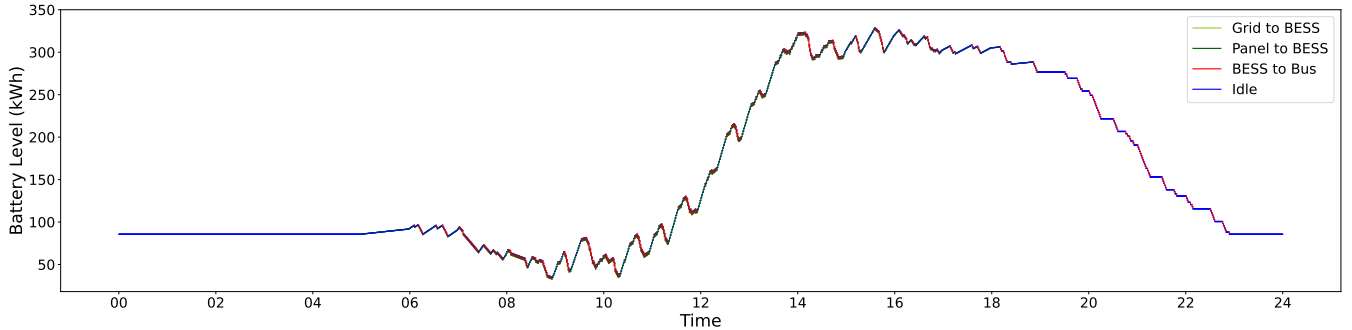
postprocessing step by assuming that energy sourced from the grid is spent first. Note that because we use a time discretization of one minute for short-term charging decisions, we do not split charging activities that draw energy from both sources within the one-minute interval. A clear trend emerges in all schedules, showing a preference for using solar energy over charging from the grid during the daytime. Additionally, the model optimizes the schedule based on peak-hour pricing, which varies across scenarios. (For Durham, peak and off-peak hours differ in summers and winters.)

For each network, the number of buses and bus-to-trip assignments varies depending on the type of scenario. For Canberra, schedule 11b rarely relies on charging from the grid during peak hours, schedule 11d uses grid charging during off-peak hours, and schedule 11f relies entirely on solar energy during peak and off-peak hours. A similar pattern, though less pronounced, can be observed in the Durham schedules due to reduced solar capacity and cheaper ToU pricing.

Figures 12a and 12b depict the system’s total energy consumption across all 52 weeks/scenarios. As previously discussed, the energy requirements for both networks depend on the temperature variations across scenarios. Also, the energy drawn from the grid or BESS fluctuates based on each scenario’s GTI and temperature characteristics. A high amount of solar energy is captured during the summer for Durham (mid-year) and Canberra (at the start and end of the year). The contribution of renewables to the total energy requirement was 37.82% and 41.38% for the Durham and Canberra networks, respectively. Figures 13a and 13b illustrates the energy utilization at a given charging location for both networks across different scenarios. The trend is similar to the overall operations discussed in the Gantt charts. The maximum energy requirement in any time step is different across scenarios. These spikes can occur when the timetables and bus-to-trip assignments are such that multiple buses arrive at the charging station simultaneously. Figures 14a and 14b show the variation of BESS energy levels across different times-of-the-day in week 50 for the Durham and Canberra networks, respectively. The blue lines indicate no change in the energy levels. Three energy transfer activities can occur every minute: from the solar panel to BESS (dark green), from the grid to BESS (light green), and from BESS to buses (red). Since we use a time discretization of one minute, for visualization purposes, we assume that these events occur sequentially, with each lasting 20 seconds, and show them separately in these figures. We notice that grid and solar power are used to charge the BESS in Durham for the selected location. However, for the Canberra network, only solar power is used to charge the BESS.



(a) Durham – (Location 35)



(b) Canberra – (Location 21)

Figure 14: BESS energy levels for week 50 for Durham (top) and Canberra (bottom)

6 Conclusions and Future Work

This study introduced a two-stage multi-scenario model to determine the charging schedules of EBs using energy from both a conventional grid and a solar-powered system. We addressed the seasonality in solar energy generation and variations in trip energy consumption due to changes in ambient temperature within a day. The first stage, or planning-level decisions, involved determining the optimal power capacity for charging stations, the area of solar panels to be installed, and the capacity of the BESS at the charging stations. The second stage, or operational-level, decisions were scenario-specific. They determined the energy transferred to EBs within a day at each time step at different charging locations either from the grid, the BESS, or both. The BESS can store energy from the solar panels or the grid. A concurrent scheduler-based algorithm was used to obtain scenario-specific bus-to-trip assignment schedules, which were used as an input to the CSP. A Charge-And-Go priority scheme was assumed, where buses preferred charging at the current trip’s end-stop rather than the next trip’s start-stop. Charging rates were assumed to be piecewise constant across time steps, and partial charging was permitted. Case studies conducted on two real-world bus transit networks, Durham and Canberra, considering RES and seasonal ToU electricity prices, demonstrated significant cost savings of 16.48% and 32.00%, respectively. Due to the block diagonal structure of the problem, we solved the CSP using Benders’ decomposition and compared its performance with that of the dual simplex method.

Our scenario-based LP model effectively captured the seasonal variations in RES, offering a more accurate representation of real-world conditions. Future research could explore non-linear charging profiles, bus battery drive cycles, and online decision-making with delays in trip schedules. Additionally, technological advancements, such as bidirectional charging, could be a valuable feature to add to our model. Nonetheless, our study provides strong support for integrating renewable energy and adapting to power generation fluctuations in the charge scheduling of electric bus fleets.

Acknowledgments

The authors thank the Ministry of Education for supporting this study through the Scheme for Transformational and Advanced Research in Sciences (STARS2/2023-0252) project titled *Efficient Algorithms for Large-Scale Public Transit Planning*.

CRedit authorship contribution statement

Madhusudan Baldua, Rito Brata Nath: Methodology, Software, Writing – Original Draft, Data Curation, Investigation, Visualization; **Vivek Vasudeva:** Software, Investigation, Writing - Review & Editing; **Tarun Rambha:** Conceptualization, Methodology, Investigation, Writing - Review & Editing, Supervision.

Appendix A Glossary

Table 10: List of abbreviations

| Acronym | Description |
|---------|--|
| EBs | Electric Buses |
| EVs | Electric Vehicles |
| EVSP | Electric Vehicle Scheduling Problem |
| CSP | Charge Scheduling Problem |
| MDVSP | Multi-Depot Vehicle Scheduling Problem |
| ToU | Time-of-Use |
| RES | Renewable Energy Sources |
| PVs | Photo-Voltaics |
| GTI | Global Tilted Irradiance |
| BESS | Battery Energy Storage System |
| LP | Linear Programming |
| CS | Concurrent Scheduler |
| NREL | National Renewable Energy Laboratory |
| MILPs | Mixed-Integer Linear Programs |
| MDP | Markov Decision Process |
| CAG | Charge-and-Go |
| GTFS | General Transit Feed Specification |
| DoD | Depth-of-Discharge |
| SoC | State-of-Charge |

References

- [1] P. Jaramillo, S. Kahn Ribeiro, P. Newman, S. Dhar, O. E. Diemuodeke, T. Kajino, D. S. Lee, S. B. Nugroho, X. Ou, A. Hammer Strømman, *et al.*, “Transport (Chapter 10),” 2022.
- [2] IEA, “Global CO2 emissions from trucks and buses in the net zero scenario, 2000-2030.” <https://www.iea.org/data-and-statistics/charts/global-co2-emissions-from-trucks-and-buses-in-the-net-zero-scenario-2000-2030>, 2023. Accessed 02-December-2023.
- [3] IEA, “Electric bus registrations and sales share by region, 2015-2022.” <https://www.iea.org/data-and-statistics/charts/electric-bus-registrations-and-sales-share-by-region-2015-2022>, 2023. Accessed 02-December-2023.
- [4] H. Hu, B. Du, W. Liu, and P. Perez, “A joint optimisation model for charger locating and electric bus charging scheduling considering opportunity fast charging and uncertainties,” *Transportation Research Part C: Emerging Technologies*, vol. 141, p. 103732, 2022.
- [5] X. Shaobo, Z. Qiankun, H. Xiaosong, L. Yonggang, and L. Xianke, “Battery sizing for plug-in hybrid electric buses considering variable route lengths,” *Energy*, vol. 226, p. 120368, 2021.
- [6] National Renewable Energy Laboratory, “Reliable future grid with more wind and solar.” <https://www.nrel.gov/docs/fy24osti/87298.pdf>, 2024. Accessed 02-December-2023.
- [7] A. Hassoune, M. Khafallah, A. Mesbahi, and D. Breuil, “Electrical design of a photovoltaic-grid system for electric vehicles charging station,” in *2017 14th International Multi-Conference on Systems, Signals & Devices (SSD)*, pp. 228–233, IEEE, 2017.
- [8] P. Newman, “Cool planning: How urban planning can mainstream responses to climate change,” *Cities*, vol. 103, p. 102651, 2020.
- [9] Enerdata Yearbook, “Share of renewables in electricity production.” <https://yearbook.enerdata.net/renewables/renewable-in-electricity-production-share.html>, 2024. Accessed 02-August-2024.
- [10] Y. Liu, Q. Zhang, C. Lyu, and Z. Liu, “Modelling the energy consumption of electric vehicles under uncertain and small data conditions,” *Transportation Research Part A: Policy and Practice*, vol. 154, pp. 313–328, 2021.

- [11] H. Jin, S. Lee, S. H. Nengroo, and D. Har, “Development of charging/discharging scheduling algorithm for economical and energy-efficient operation of multi-EV charging station,” *Applied Sciences*, vol. 12, no. 9, p. 4786, 2022.
- [12] S. S. Perumal, R. M. Lusby, and J. Larsen, “Electric bus planning & scheduling: A review of related problems and methodologies,” *European Journal of Operational Research*, vol. 301, no. 2, pp. 395–413, 2022.
- [13] C. Yang, W. Lou, J. Yao, and S. Xie, “On charging scheduling optimization for a wirelessly charged electric bus system,” *IEEE Transactions on Intelligent Transportation Systems*, vol. 19, no. 6, pp. 1814–1826, 2017.
- [14] M. Alonso, H. Amaris, J. G. Germain, and J. M. Galan, “Optimal charging scheduling of electric vehicles in smart grids by heuristic algorithms,” *Energies*, vol. 7, no. 4, pp. 2449–2475, 2014.
- [15] S. Deb, K. Tammi, K. Kalita, and P. Mahanta, “Impact of electric vehicle charging station load on distribution network,” *Energies*, vol. 11, no. 1, p. 178, 2018.
- [16] N. Korolko and Z. Sahinoglu, “Robust optimization of EV charging schedules in unregulated electricity markets,” *IEEE Transactions on Smart Grid*, vol. 8, no. 1, pp. 149–157, 2015.
- [17] L. Jian, Y. Zheng, and Z. Shao, “High efficient valley-filling strategy for centralized coordinated charging of large-scale electric vehicles,” *Applied Energy*, vol. 186, pp. 46–55, 2017.
- [18] Y. Zhou, H. Wang, Y. Wang, and R. Li, “Robust optimization for integrated planning of electric-bus charger deployment and charging scheduling,” *Transportation Research Part D: Transport and Environment*, vol. 110, p. 103410, 2022.
- [19] N. Qin, A. Gusrialdi, R. P. Brooker, T. Ali, *et al.*, “Numerical analysis of electric bus fast charging strategies for demand charge reduction,” *Transportation Research Part A: Policy and Practice*, vol. 94, pp. 386–396, 2016.
- [20] R.-C. Leou and J.-J. Hung, “Optimal charging schedule planning and economic analysis for electric bus charging stations,” *Energies*, vol. 10, no. 4, p. 483, 2017.
- [21] Y. He, Z. Liu, and Z. Song, “Optimal charging scheduling and management for a fast-charging battery electric bus system,” *Transportation Research Part E: Logistics and Transportation Review*, vol. 142, p. 102056, 2020.
- [22] M. Dietmannsberger, M. Schumann, M. Meyer, and D. Schulz, “Modelling the electrification of bus depots using real data: Consequences for the distribution grid and operational requirements,” in *1st E-Mobility Power System Integration Symposium*, p. 8, 2017.
- [23] A. Jahic, M. Eskander, and D. Schulz, “Charging schedule for load peak minimization on large-scale electric bus depots,” *Applied Sciences*, vol. 9, no. 9, p. 1748, 2019.
- [24] A. Houbbadi, R. Trigui, S. Pelissier, E. Redondo-Iglesias, and T. Bouton, “Optimal scheduling to manage an electric bus fleet overnight charging,” *Energies*, vol. 12, no. 14, p. 2727, 2019.
- [25] A. Abdelwahed, P. L. van den Berg, T. Brandt, J. Collins, and W. Ketter, “Evaluating and optimizing opportunity fast-charging schedules in transit battery electric bus networks,” *Transportation Science*, vol. 54, no. 6, pp. 1601–1615, 2020.
- [26] Y. He, Z. Liu, and Z. Song, “Joint optimization of electric bus charging infrastructure, vehicle scheduling, and charging management,” *Transportation Research Part D: Transport and Environment*, vol. 117, p. 103653, 2023.
- [27] Y. Wang, F. Liao, J. Bi, and C. Lu, “Optimal battery electric bus system planning considering heterogeneous vehicles, opportunity charging, and battery degradation,” *Renewable Energy*, vol. 237, p. 121596, 2024.
- [28] R. B. Nath, T. Rambha, and M. Schiffer, “On the impact of co-optimizing station locations, trip assignment, and charging schedules for electric buses,” *Transportation Research Part C: Emerging Technologies*, vol. 167, p. 104839, 2024.
- [29] L. Yao, Z. Damiran, and W. H. Lim, “Optimal charging and discharging scheduling for electric vehicles in a parking station with photovoltaic system and energy storage system,” *Energies*, vol. 10, no. 4, p. 550, 2017.

- [30] R. Fachrizal, M. Shepero, D. van der Meer, J. Munkhammar, and J. Widén, “Smart charging of electric vehicles considering photovoltaic power production and electricity consumption: A review,” *eTransportation*, vol. 4, p. 100056, 2020.
- [31] Y. He, Z. Song, and Z. Liu, “Fast-charging station deployment for battery electric bus systems considering electricity demand charges,” *Sustainable Cities and Society*, vol. 48, p. 101530, 2019.
- [32] L. Zhong, Z. Zeng, Z. Huang, X. Shi, and Y. Bie, “Joint optimization of electric bus charging and energy storage system scheduling,” *Frontiers of Engineering Management*, pp. 1–21, 2024.
- [33] J.-T. Liao, H.-W. Huang, H.-T. Yang, and D. Li, “Decentralized V2G/G2V scheduling of EV charging stations by considering the conversion efficiency of bidirectional chargers,” *Energies*, vol. 14, no. 4, p. 962, 2021.
- [34] B.-R. Ke, Y.-H. Lin, H.-Z. Chen, and S.-C. Fang, “Battery charging and discharging scheduling with demand response for an electric bus public transportation system,” *Sustainable Energy Technologies and Assessments*, vol. 40, p. 100741, 2020.
- [35] J. Yusuf, A. J. Hasan, J. Garrido, S. Ula, and M. J. Barth, “A comparative techno-economic assessment of bidirectional heavy duty and light duty plug-in electric vehicles operation: A case study,” *Sustainable Cities and Society*, vol. 95, p. 104582, 2023.
- [36] B. Singh, A. Verma, A. Chandra, and K. Al-Haddad, “Implementation of solar PV-battery and diesel generator based electric vehicle charging station,” *IEEE Transactions on Industry Applications*, vol. 56, no. 4, pp. 4007–4016, 2020.
- [37] Y. Li, X. Li, C. Zhang, and Y. Zhang, “Optimizing the photovoltaic-assisted electric bus network with rooftop energy supply,” *Renewable Energy*, vol. 234, p. 121244, 2024.
- [38] D. Li, A. Zouma, J.-T. Liao, and H.-T. Yang, “An energy management strategy with renewable energy and energy storage system for a large electric vehicle charging station,” *eTransportation*, vol. 6, p. 100076, 2020.
- [39] N. Kumar, T. Kumar, S. Nema, and T. Thakur, “A multiobjective planning framework for EV charging stations assisted by solar photovoltaic and battery energy storage system in coupled power and transportation network,” *International Journal of Energy Research*, vol. 46, no. 4, pp. 4462–4493, 2022.
- [40] X. Liu, X. Liu, X. Zhang, Y. Zhou, J. Chen, and X. Ma, “Optimal location planning of electric bus charging stations with integrated photovoltaic and energy storage system,” *Computer-Aided Civil and Infrastructure Engineering*, vol. 38, no. 11, pp. 1424–1446, 2023.
- [41] X. Liu, S. Yeh, P. Plötz, W. Ma, F. Li, and X. Ma, “Electric bus charging scheduling problem considering charging infrastructure integrated with solar photovoltaic and energy storage systems,” *Transportation Research Part E: Logistics and Transportation Review*, vol. 187, p. 103572, 2024.
- [42] T. Zhang, W. Chen, Z. Han, and Z. Cao, “Charging scheduling of electric vehicles with local renewable energy under uncertain electric vehicle arrival and grid power price,” *IEEE Transactions on Vehicular Technology*, vol. 63, no. 6, pp. 2600–2612, 2013.
- [43] P. Zhuang and H. Liang, “Stochastic energy management of electric bus charging stations with renewable energy integration and B2G capabilities,” *IEEE Transactions on Sustainable Energy*, vol. 12, no. 2, pp. 1206–1216, 2020.
- [44] D. Huang and S. Wang, “A two-stage stochastic programming model of coordinated electric bus charging scheduling for a hybrid charging scheme,” *Multimodal Transportation*, vol. 1, no. 1, p. 100006, 2022.
- [45] S. Rafique, M. Nizami, U. Irshad, M. Hossain, and S. Mukhopadhyay, “A two-stage multi-objective stochastic optimization strategy to minimize cost for electric bus depot operators,” *Journal of Cleaner Production*, vol. 332, p. 129856, 2022.
- [46] J. Soares, B. Canizes, M. A. F. Ghazvini, Z. Vale, and G. K. Venayagamoorthy, “Two-stage stochastic model using Benders’ decomposition for large-scale energy resource management in smart grids,” *IEEE Transactions on Industry Applications*, vol. 53, no. 6, pp. 5905–5914, 2017.
- [47] A. Najafi, K. Gao, O. Parishwad, G. Tsaousoglou, S. Jin, and W. Yi, “Integrated optimization of charging infrastructure, electric bus scheduling and energy systems,” *Transportation Research Part D: Transport and Environment*, vol. 141, p. 104664, 2025.

- [48] S. M. Arif, T. T. Lie, B. C. Seet, S. M. Ahsan, and H. A. Khan, “Plug-in electric bus depot charging with PV and ESS and their impact on LV feeder,” *Energies*, vol. 13, no. 9, p. 2139, 2020.
- [49] J. A. Manzolli, J. P. F. Trovao, and C. H. Antunes, “Electric bus coordinated charging strategy considering V2G and battery degradation,” *Energy*, vol. 254, p. 124252, 2022.
- [50] A. M. Geoffrion, “Generalized Benders decomposition,” *Journal of Optimization Theory and Applications*, vol. 10, pp. 237–260, 1972.
- [51] R. Rahmaniani, T. G. Crainic, M. Gendreau, and W. Rei, “The Benders decomposition algorithm: A literature review,” *European Journal of Operational Research*, vol. 259, no. 3, pp. 801–817, 2017.
- [52] C. C. Ribeiro and F. Soumis, “A column generation approach to the multiple-depot vehicle scheduling problem,” *Operations Research*, vol. 42, no. 1, pp. 41–52, 1994.
- [53] A. Hadjar, O. Marcotte, and F. Soumis, “A branch-and-cut algorithm for the multiple depot vehicle scheduling problem,” *Operations Research*, vol. 54, no. 1, pp. 130–149, 2006.
- [54] A. A. Bertossi, P. Carraresi, and G. Gallo, “On some matching problems arising in vehicle scheduling models,” *Networks*, vol. 17, no. 3, pp. 271–281, 1987.
- [55] J. D. Adler and P. B. Mirchandani, “The vehicle scheduling problem for fleets with alternative-fuel vehicles,” *Transportation Science*, vol. 51, no. 2, pp. 441–456, 2017.
- [56] E. Yao, T. Liu, T. Lu, and Y. Yang, “Optimization of electric vehicle scheduling with multiple vehicle types in public transport,” *Sustainable Cities and Society*, vol. 52, p. 101862, 2020.
- [57] G.-J. Zhou, D.-F. Xie, X.-M. Zhao, and C. Lu, “Collaborative optimization of vehicle and charging scheduling for a bus fleet mixed with electric and traditional buses,” *IEEE Access*, vol. 8, pp. 8056–8072, 2020.
- [58] M. Wen, E. Linde, S. Ropke, P. Mirchandani, and A. Larsen, “An adaptive large neighborhood search heuristic for the electric vehicle scheduling problem,” *Computers & Operations Research*, vol. 76, pp. 73–83, 2016.
- [59] L. Bodin, D. Rosenfield, and A. Kydes, “UCOST: a micro approach to a transportation planning problem,” *Journal of Urban Analysis*, vol. 5, no. 1, 1978.
- [60] O. Sadeghian, A. Oshnoei, B. Mohammadi-Ivatloo, V. Vahidinasab, and A. Anvari-Moghaddam, “A comprehensive review on electric vehicles smart charging: Solutions, strategies, technologies, and challenges,” *Journal of Energy Storage*, vol. 54, p. 105241, 2022.
- [61] F. Vivas, F. Segura, J. Andújar, A. Calderón, and F. Isorna, “Battery-based storage systems in high voltage-DC bus microgrids. a real-time charging algorithm to improve the microgrid performance,” *Journal of Energy Storage*, vol. 48, p. 103935, 2022.
- [62] S. Coelho, V. Monteiro, T. J. Sousa, L. A. Barros, D. Pedrosa, C. Couto, and J. L. Afonso, “A unified power converter for solar PV and energy storage in DC microgrids,” *Batteries*, vol. 8, no. 10, p. 143, 2022.
- [63] J. A. Tejero-Gómez and Á. A. Bayod-Rújula, “Analysis of photovoltaic plants with battery energy storage systems (PV-BESS) for monthly constant power operation,” *Energies*, vol. 16, no. 13, p. 4909, 2023.
- [64] K. Mannepalli, K. Vinoth, S. K. Mohapatra, R. Rahul, D. P. Gangodkar, A. Madduri, M. Ravichandran, R. Sathyamurthy, and V. Mohanavel, “Allocation of optimal energy from storage systems using solar energy,” *Energy Reports*, vol. 8, pp. 836–846, 2022.
- [65] J. Ji, Y. Bie, Z. Zeng, and L. Wang, “Trip energy consumption estimation for electric buses,” *Communications in Transportation Research*, vol. 2, p. 100069, 2022.
- [66] NREL, “Best practices handbook for the collection and use of solar resource data for solar energy applications: Third edition.” <https://www.nrel.gov/docs/fy21osti/77635.pdf>, 2021. Page 238.
- [67] B. Hardman, “Life Expectancy of Battery Storage Systems.” <https://ecoaffect.org/battery-storage/life-expectancy-battery-storage-systems/>, 2024. [Online; accessed 25-January-2025].

- [68] H. Rallo, L. C. Casals, D. De La Torre, R. Reinhardt, C. Marchante, and B. Amante, “Lithium-ion battery 2nd life used as a stationary energy storage system: Ageing and economic analysis in two real cases,” *Journal of Cleaner Production*, vol. 272, p. 122584, 2020.
- [69] A. Lajunen, “Lifecycle costs and charging requirements of electric buses with different charging methods,” *Journal of Cleaner Production*, vol. 172, pp. 56–67, 2018.
- [70] K. Gamble, “Aging Gracefully: How NREL Is Extending the Lifetime of Solar Modules.” <https://www.nrel.gov/news/features/2022/aging-gracefully-how-nrel-is-extending-the-lifetime-of-solar-modules.html>, 2022. [Online; accessed 25-January-2025].
- [71] J. R. Birge and F. Louveaux, *Introduction to Stochastic Programming*. New York, NY, USA: Springer-Verlag, 1997.
- [72] Rylan Urban, “Solar power Ontario (2024 guide).” <https://www.energyhub.org/ontario/>, 2023. Accessed 25-January-2025.
- [73] Australian Government, “Size your solar system.” <https://www.energy.gov.au/solar/solar-system-design/size-your-solar-system>, 2023. Accessed 25-January-2025.
- [74] National Renewable Energy Laboratory, “U.S. solar photovoltaic system and energy storage cost benchmarks, with minimum sustainable price analysis: Q1 2023.” <https://www.nrel.gov/docs/fy23osti/87303.pdf>, 2023. Accessed 25-January-2025.
- [75] Alectra Utilities, “Time-of-Use Pricing.” <https://alectrautilities.com/time-use-pricing>, 2025. [Online; accessed 25-January-2025].
- [76] Australian Energy Regulator, “Business Saver time-of-use 2.0.” <https://www.energymadeeasy.gov.au/plan?id=ACT705815MBE3&postcode=2601>, 2024. [Online; accessed 25-January-2025].
- [77] M. Stumpe, D. Rößler, G. Schryen, and N. Kliewer, “Study on sensitivity of electric bus systems under simultaneous optimization of charging infrastructure and vehicle schedules,” *EURO Journal on Transportation and Logistics*, vol. 10, p. 100049, 2021.
- [78] S. M. B. Sadati, J. Moshtagh, M. Shafie-khah, A. Rastgou, and J. P. Catalão, “Operational scheduling of a smart distribution system considering electric vehicles parking lot: A bi-level approach,” *International Journal of Electrical Power & Energy Systems*, vol. 105, pp. 159–178, 2019.
- [79] F. A. Tiano, G. Rizzo, M. Marino, and A. Monetti, “Evaluation of the potential of solar photovoltaic panels installed on vehicle body including temperature effect on efficiency,” *eTransportation*, vol. 5, p. 100067, 2020.
- [80] National Renewable Energy Laboratory, “Cost projections for utility-scale battery storage: 2023 update.” <https://www.nrel.gov/docs/fy23osti/85332.pdf>, 2023. Accessed 25-January-2025.
- [81] N. Dirks, M. Schiffer, and G. Walther, “On the integration of battery electric buses into urban bus networks,” *Transportation Research Part C: Emerging Technologies*, vol. 139, p. 103628, 2022.
- [82] TLS Offshore Containers / TLS Energy, “Understanding Battery Energy Storage Systems: Power Capacity, Energy Capacity, and C-Rates.” <https://www.tls-containers.com/tls-blog/understanding-bess-mw-mwh-and-chargingdischarging-speeds-1c-05c-025c>, 2024. [Online; accessed 25-January-2025].
- [83] CanadianSolar, “Utility Scale Energy Storage.” https://static.csisolar.com/wp-content/uploads/2021/01/14093918/CanadianSolar_CSES351A6-3500KVA-14MWH-BESS-r7_J1.pdf, 2021. [Online; accessed 25-January-2025].